



Studying of the fluid's property adjustment and its application in metal foam industry

Dissertation Thesis

Study programme:

P2302 Machines and Equipment

Study branch:

Machine and Equipment Design

Author:

Ing. Shehab Hassan Attia

Thesis Supervisor:

prof. Ing. Karel Fraňa, Ph.D.

Department of Power Engineering Equipment



Declaration

I hereby certify, I, myself, have written my dissertation as an original and primary work using the literature listed below and consulting it with my thesis supervisor and my thesis counsellor.

I acknowledge that my dissertation is fully governed by Act No. 121/2000 Coll., the Copyright Act, in particular Article 60 – School Work.

I acknowledge that the Technical University of Liberec does not infringe my copyrights by using my dissertation for internal purposes of the Technical University of Liberec.

I am aware of my obligation to inform the Technical University of Liberec on having used or granted license to use the results of my dissertation; in such a case the Technical University of Liberec may require reimbursement of the costs incurred for creating the result up to their actual amount.

At the same time, I honestly declare that the text of the printed version of my dissertation is identical with the text of the electronic version uploaded into the IS/STAG.

I acknowledge that the Technical University of Liberec will make my dissertation public in accordance with paragraph 47b of Act No. 111/1998 Coll., on Higher Education Institutions and on Amendment to Other Acts (the Higher Education Act), as amended.

I am aware of the consequences which may under the Higher Education Act result from a breach of this declaration.

February 16, 2022

Ing. Shehab Hassan Attia

Acknowledgments

I would like to thank the following people, without whom I would not have been able to complete this research, and without whom I would not have made it through my PhD degree.

I would like to thank my PhD supervisor Prof. Ing. Karel Fraňa, Ph.D. for guiding and supporting my research work, prof. Ing. Iva Nová, CSc. for her support with the Hybrid Materials for Hierarchical Structures project, lab results and collaborating on the topic of Metal foam. doc. Ing. Petra Dančová, Ph.D. for accomodating my research needs with access and usage of the university lab also I am thankful for the Technical univesity of Dresden for accomidating me on one of my interships for studying CFD, as well as Brandenburg technical university for hosting me for my second internship.

This work was supported by the Ministry of Education, Youth and Sports of the Czech Republic and the European Union - European Structural and Investment Funds in the frames of Operational Programme Research, Development and Education - project Hybrid Materials for Hierarchical Structures (HyHi, Reg. No. CZ.02.1.01/0.0/0.0/16_019/0000843).

Abstract

The main aim of this study is to find criteria influencing the shapes of a gas bubbles rising in stagnant liquid experimentally to form foam. A testing facility with the high-speed camera was designed. The results obtained are presented in terms of dimensionless parameters i.e. Reynolds's, Morton's and Eötvös. Factors varied to test their dependency such as nozzle diameter (3 – 5 mm), rate of flow rate (15 and 130 l/h), viscosity, surface tension and density were changed in order to see their effect on the shape of the bubble, its velocity in the liquid, surface tension force, drag force and buoyancy force. In order to vary such parameters a water-ethanol mixture was used in the tank. Also the foam formed was examined using water ethanol mixture in predicting the Foam bubble behavior in multiphase flow. The study compares the concept of formation of foam at the surface of the mixture with the procedure of producing aluminium foam by direct gas injection. Material properties such as kinematic viscosity, density and surface tension on the foaming process will be studied experimentally, while the foam bubble size will be studied by means of digital image processing, finally the study proposes a concept for production of metal foam and experiments performed in Technical university of Liberec

Index Keywords: Metal Foam, Hierarchical materials, Ethanol Foam model

Contents

| | |
|---|----|
| Abstract | 4 |
| 1 Introduction and background | 9 |
| 1.1 Research goal..... | 9 |
| 1.2 Theory behind Foam bubbles | 10 |
| 1.2.1 Surface tension | 10 |
| 1.2.2 Gravity vs surface tension forces..... | 10 |
| 1.2.3 Young laplace equation:..... | 11 |
| 1.2.4 Marangoni effect..... | 12 |
| 1.2.5 What is a Hierarchical material?..... | 13 |
| 1.2.6 Classification of hierarchical materials:..... | 14 |
| 1.3 Metal foam as hierarchical material..... | 15 |
| 1.4 Metal Foam Market research..... | 16 |
| 1.5 Current state of art in Metal Foam Applications | 18 |
| 1.6 Examples of available Metal Foam production equipment..... | 22 |
| 1.6.1 Foaming of metals by direct gas injection (Hydro/Alcan):..... | 22 |
| 1.6.2 Metal foam production by gas agents | 26 |
| 1.6.3 Metal Foam by Mold Casting..... | 28 |
| 1.6.4 Metal Foam production investment casting | 29 |
| 1.6.5 Challenges and opportunities | 29 |
| 1.6.6 Metal foam by compression | 30 |

| | | |
|-------|--|----|
| 2 | Experiment Set-up | 32 |
| 3 | Methodology | 34 |
| 3.1 | Idea of a foaming model..... | 34 |
| 3.1.1 | Comparison between the Foam Model and Aluminium Model: | 35 |
| 3.2 | Image acquisition equipment..... | 35 |
| 3.3 | Viscosity Meter | 36 |
| 3.4 | Surface Tension Meter (Bubble pressure tension-meter):..... | 38 |
| 3.5 | Image processing software | 39 |
| 3.6 | Flow meter..... | 42 |
| 3.7 | Air compressor..... | 43 |
| 3.8 | Dimensionless Parameters..... | 43 |
| 3.8.1 | Morton number | 43 |
| 3.8.2 | Eötvös number | 44 |
| 3.8.3 | Reynolds number | 44 |
| 4 | Results and Discussion | 46 |
| 4.1 | Water with Nozzle diameter is 3mm and $v = 15$ l/h [D3V15] | 46 |
| 4.1.1 | Bubble shapes..... | 46 |
| 4.1.2 | Monitoring the effect of a higher flowrate..... | 50 |
| 4.1 | Comparison between D5V130 and D3V15:..... | 51 |
| 4.1.1 | Comparison to similar studies: | 53 |

| | | |
|-------|--|----|
| 4.2 | Water-Ethanol mixture with the nozzle diameter of 3mm and $v = 15$ l/h | 54 |
| 4.3 | Analysis for produced Foam in water Ethanol mixture | 59 |
| 4.3.1 | Effect of Molar Fraction of Ethanol on the foamability of the mixture: | 59 |
| 4.3.2 | Flow rate effect on foam size: | 60 |
| 4.3.3 | Digital Image processing..... | 60 |
| 4.3.4 | Foam Analysis experiment..... | 65 |
| 4.3.5 | Analysis uncertainties: | 67 |
| 4.4 | CFD Study for bubble under the surface..... | 68 |
| 4.4.1 | Boundary conditions | 70 |
| 4.4.2 | Results (volume fraction contours):..... | 73 |
| 4.4.3 | Simulation Model validation (Bubble diameter):..... | 75 |
| 4.4.4 | Effect of flow rate on foam pore size..... | 77 |
| 5 | Equipment Design Concept for Metal foam Production | 79 |
| 5.1 | Operation conditions:..... | 80 |
| 5.2 | Components Created:..... | 82 |
| 5.2.1 | Molten Metal tank:..... | 82 |
| 5.2.2 | Propeller | 82 |
| 5.2.3 | Nozzle mesh plate..... | 83 |
| 5.2.4 | Conveyor belt | 84 |

| | | |
|---|---|-----|
| 6 | Metal Foam prepared at TUL | 84 |
| 7 | Conclusion | 89 |
| 8 | List of Figures | 92 |
| 9 | Bibliography | 97 |
| | Appendix 1 – CFD Air Bubble volume fraction contours: | 106 |
| | Appendix 2 – High Speed Camera Air Bubble photos: | 112 |

1 Introduction and background

1.1 Research goal

This PhD thesis is concerned with the possibility of using water ethanol mixture as a metal foam model, to aid in predicting the bubble behavior in multiphase flow, the study compares bubble shape parameters like Aspect Ratio, Morton number and Eötvös number to corresponding parameters in the production of Aluminum metal foam by direct gas injection. The effect of the different material properties such as kinematic viscosity, density and surface tension on the foaming process will be studied experimentally. Also a CFD simulation to be carried out to predict the behavior of a gas bubble under the surface of liquid. Acquisition of this practical knowledge can improve the effectiveness of the real foaming process of the aluminum and aluminum alloys. Simultaneously, it helps to understand main basic features of the formed metal foams. The experimental study used a speed camera to capture the shape of gas bubble under the liquid surface, and by using Image processing bubble parameters are acquired through different time steps, more over this was repeated several instances for different viscosity and surface tension values, while obtaining Morton, Eötvös and Reynolds numbers, to define the best parameters for the foaming process for water-ethanol mixture, such results are to be compared to their corresponding parameters for the direct injection foaming method for aluminum, with the main aim to be able to propose best foaming conditions for metal foam, in means to decreasing time and cost required to produce aluminum metal foam through test trials, the research would test such parameters it would be possible to predict properties of aluminum foam from the safety of a normal lab, with no need for heating furnace or X ray vision equipment to monitor the bubble parameters in liquid aluminum.

1.2 Theory behind Foam bubbles

1.2.1 Surface tension

Is a phenomenon that happens at the interface between either 2 fluids or fluid and surface, typical situation could be water and air, thermodynamically for water molecules it's better to hold together than to be in contact with air molecules, the water molecules will minimize the surface area in contact of air, creating a water droplet in the shape of a sphere, same thing could be seen on surfaces, like wax and a drop of water, such materials are given the name hydrophobic. The other extreme would be a surface that would spread the water, so water molecules would rather be in touch with the surface, and such substances are given the name hydrophilic surfaces

Surface tension inherently is work associated with increasing the contact area between 2 fluids, it could be described as Energy per surface area, or the force per length

$$\gamma = \frac{E}{A} = \frac{F}{L} \quad \left(\frac{N}{m}\right) \quad (1.1)$$

Where γ is surface tension, E is energy, A is area, F is force and L is length.

1.2.2 Gravity vs surface tension forces

Surface tension is a function of Area, so it depends on square the characteristic length L^2 Gravity for comparison is a body force and it depends on the volume of an object, so in this case L^3

This observation is important because for large sized objects the gravity force is way more important than surface tension forces, As we go to smaller length scales in this case surface tension forces becomes more influential

1.2.3 Young laplace equation:

Surface tension is work needed to increase interfacial area between 2 fluids, or a fluid and a solid, the interfacial area is bordered by 2 radii R1 and R2 (depicted in Figure 1), with an arc length of x, y and z respectively, and causing a change of $\partial x, \partial y$ and ∂z due to expansion:

$$\gamma \partial w = \gamma \partial A \quad (1.2)$$

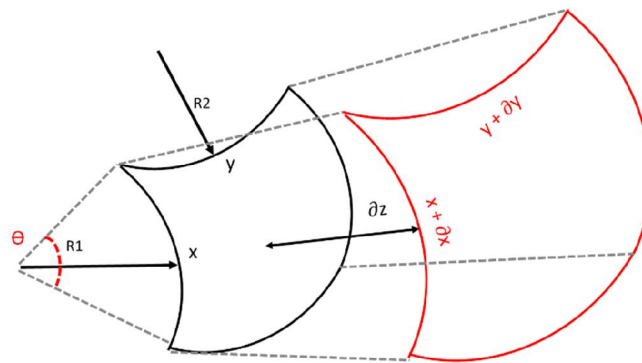


Figure 1 increase of radii due to interfacial expansion between 2 fluids

Work to increase the change in the area could be described by a curved line, assuming a fluid bubble expanded, the change of area would be: $\partial A = A_f - A_i$

$$\partial A = A_f - A_i$$

$$\partial A = (x + \partial x)(y + \partial y) - xy$$

$$= xy + x\partial y + y\partial x + \partial x \partial y - xy$$

$$\partial w = \gamma (x \partial y + y \partial x) \quad (1.3)$$

Change in the bubble size could also correspond to pressure and volume change:

$$\partial w = \Delta P x y \partial z \quad (1.4)$$

From Trigonometric symmetry, from Figure 1:

$$\theta = \frac{x + \partial x}{R_1 + \partial z} = \frac{x}{R_1}$$

$$\partial x = \frac{x \partial z}{R_1}$$

Similarly:

$$\partial y = \frac{y \partial z}{R_2}$$

Equations (1.3) = (1.4)

$$\gamma (x \partial y + y \partial x) = \Delta P x y \partial z$$

$$\Delta P = \gamma \left(\frac{1}{R_1} + \frac{1}{R_2} \right) \quad (1.5)$$

1.2.4 Marangoni effect

An interesting phenomenon due to surface tension is Marangoni effect, if you put a drop of water with alcohol it starts to defragment and decompose, the entire solution start to form a sea of tiny droplets, this is due to a surface gradient of surface tension, water usually resists being separated this allows insects to rest on water, another example could be seen in alcohol mixtures, usually alcohol evaporates, it's concentration in the thin film decreases, this causes a gradient in surface tension, which cause a non-equilibrium state of

forces tangent to the container surface, causing the liquid to ascend up the interior wall of the container, this could be seen in what is called “tears of wine” in which on the edge of the interface between wine and glass there seems to be liquid flowing down on the glass wine interface, essentially the Marangoni effect could be described as a dynamic of mass transfer along an interfacial surface due to a gradient of surface tension. A model of this effect in terms of speed of flow of the liquid when a patch with radius r [m] of surfactant is added to water [1] expressed in Equation (1.6), for γ_w surface tension of water, γ_s surface tension of the surfactant-covered water surface, μ the viscosity of water, and ρ the mass density of water

1.2.5 What is a Hierarchical material?

Hierarchical materials are organized structures of material that are inspired by existing structures and compositions in nature. It relies on repeating a certain structure or length as a pattern to cause superior properties to that of normally arranged units of such material. Such materials acquire some characteristics from the nature occurring material including structural hierarchy, responsiveness to environment like in bone, it is adaptive to repair damage, in which could be called smart in a way it detects damage and restructured itself to overcome it, and lastly hierarchical materials also adapt self-organization, which could be also a trait of smart materials.

Some of the fascinating examples for materials naturally occurring is bone which is composite of hydroxyapatite which has a multi length-scale structure hierarchy, or wood which is basically cellulose fibers in a lignin hemicellulose matrix, some other nature occurring material is purely polymeric like hair for example.

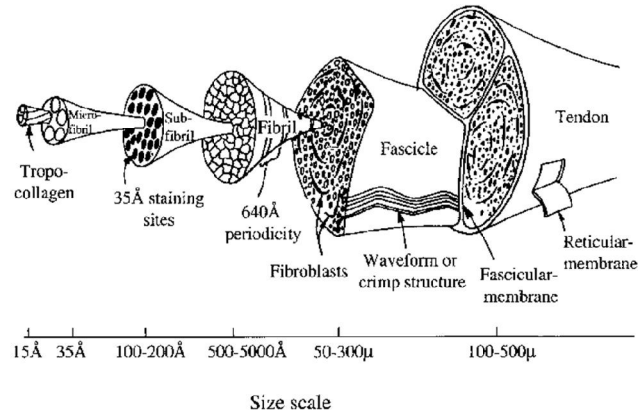


Figure 2 the structural hierarchy of ligament and tendon [85].

1.2.6 Classification of hierarchical materials:

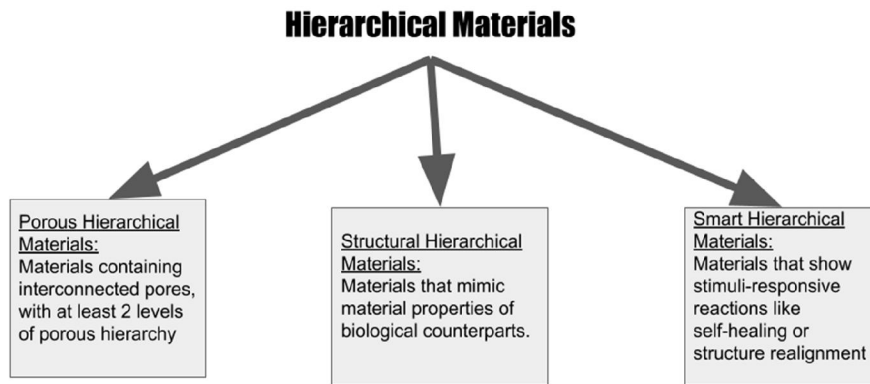


Figure 3 illustration of different types of Hierarchical Materials

When hierarchical materials are mentioned one can think of some broad groups, which is based on some basic characteristics, either Porous hierarchical materials, structural hierarchical materials or smart hierarchical materials, fig 2 illustrates the differences between the 3 main types

This research would mainly focus on Porous hierarchical materials, Hierarchical porosities offer high specific surface area and capable selectivity, efficient transportation, adsorption, and reaction route ways, among which macro porosity and mesoporosity are favorable for light propagation and photon absorption on photo catalysis. The assembly of Nano crystal building units into larger organized conformations and geometrical architectures with hierarchical porous structure is a useful way to design and control the advanced photo catalytic materials with high performance in practical applications [2]

1.3 Metal foam as hierarchical material

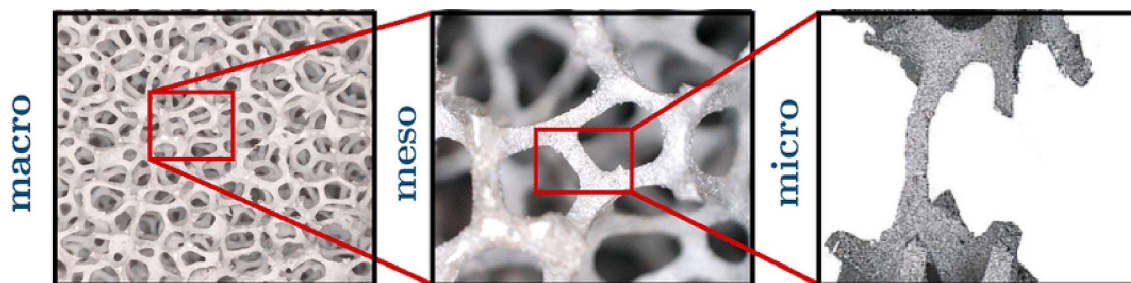


Figure 4 comparison between different metal foams [3]

The cellular structure of metal foam affects the material behaviour, the characteristic of the micro / macro structure of the metal foam highly affects the behavior in real life application [3], understanding why a certain material behave in a certain way could come mainly from studying the cell structure on several hierarchical levels, Mainly there is 3 hierarchical levels for metal foams to be studied, macro, meso and micro. Macroscopic level usually describes the material in its entirety, the next level of depth would be the mesoscopic level in this level the pores making the material are studied individually, each open cell is observed in terms of size and behaviour under stress. Finally the most indepth level of visual analysis is the microscopic, that's the level in which individual elements of the cell are examined. Analysing those hierarchical levels gives the best understanding for how materials act in that way under specific stress or strain forces.

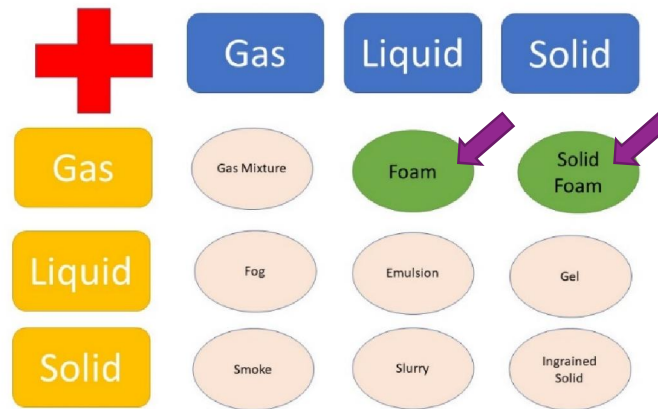


Figure 5 definition of foam

1.4 Metal Foam Market research

Metal foam has been gaining popularity recently, Market demands have pursued new material solutions catering for low specific weight, porosity, high stiffness and impact absorption, as stated by V.C. Srivastava (2006) [4]. Which makes using metal foam attractive for modern industry manufacturers, Potential uses in light weight applications including automotive, aircraft, and heat exchangers, accelerated such research from a niche solution to a currently highly commercialized utilization as surveyed by Bhatnagar (2017) [5]

The word “foam” has been used in many different connotations, thus there is a need to define it. Foam is the product of gas bubbles locked inside a liquid by the force of surface tension of that liquid. Yet as Banhart (2001) defined it, for most industrial applications the foam used would be Solid foam that has cellular form [6]. Figure 1 could be used to clarify the different types of phase mixtures and the common nomenclature describing such mixtures.

Several ways are used to manufacture metal foam, it's in continuous increase according to market trends studied by Seeliger (2012) due to market demand for lower specific weight with high stiffness for aluminium foam sandwich [7],

or ability to absorb sounds in acoustic applications due to its porous structure as stated by Jorge P. (July 2010) [8]. One main process to manufacture the foam by gas injection, in which the metal foams are directly fabricated by injecting a pressurized gas in the molten metal, for this approach several factors are considered influencing for the process to be carried out successfully for example the viscosity of the molten metal, viscosity pressure of gas injected. The viscosity of the metal is usually controlled by adding some salt or powdered ceramic like (Al₂O₃/SiC) as shown by N. Babcsan J. (2003) [9]. McKinsey & Co a management consulting company made a study that suggests increased demand for lightweight materials across several industries including aviation and passenger vehicles, the expected increase is estimated to be 70% in 2030, for comparison it used to be 30% in 2010 [10]

Currently there are studies giving satisfactory results using empirical equations to describe the shape, aspect ratio of a rising gas bubble in stagnant liquids, shapes and terminal velocities of bubbles rising in viscous liquids have been determined. Such studies were used to pave the way for this paper such as the one analysing Morton numbers (Mo) greater than 4×10^{-3} showing that the drag coefficient and dimensionless bubble shape are functions only of Reynolds number (Re) in study published by D. Bhaga in Journal of fluid Mechanics (1981) [11], or J.R. Grace (1976) that surveyed the parameters used to characterize the shape of rigid particles, and the factors that determine the shape of bubbles and drops [12]. Examples for popularly studied influencing factors are: viscosity of the liquid, surface tension, volume flow rates and nozzle diameters, using several approaches in defining main parameters for the shape of the bubbles. Several experimental studies like that of individual bubbles ca. 2.5 mm in diameter were produced at a capillary in water containing froth, polymer or inorganic salt, where bubble aspect ratio (shape) and rise velocity were measured by M. Maldonado (2013) 1.2 m above the point of generation [13]. The experimental study of the bubble trajectory in three-dimensional space that was deduced by analysing the bubble characteristics in two-dimensional plane. This was captured by a single high-

speed camera and the bubble trajectory in the water was ascertained by this method explained by Hongjie (April 2015) [14] and the experimental study of deformation of gas bubbles rising in different liquids over a wide range of Morton numbers, from 1×10^{-11} to 1, in relation to bubble diameters by . T. Maxworthy (1996) [15] all provided an image for what experimental data is available to base this study on. also numerical publications were studied, for example VOF-based numerical method for simulating mass transfer across deformable fluid interfaces, with the underlying mathematical model based on continuum thermo-mechanics, allowing for different solubilities of the species in the respective fluid phases by Dieter Bothe (September 2013) [16]. The dynamics of a bubble, initially stationary and spherical, rising in a viscous Newtonian liquid studied numerically using 3-D Volume-of-Fluid (VOF) method implemented in the Gerris flow solver by Monica Gumulya (February 2016) [17], numerical method combining the volume fraction data obtained from a primary multi-fluid simulation with simple and efficient secondary bubble simulation by Ren, B. (2015) [18] and theoretical studies like the one by A. TOMIYAMAA (2007) for analysis to determine dimensionless groups that influence single isolated gas bubble's velocity in a stagnant liquid, rising in a large container filled with different viscosity liquids [19], or on the pressure developed in a liquid during the collapse of a spherical bubble in the stagnant liquid by Lord Rayleigh in (1917) [20]. Also, studies using same dimensionless parameters that shall be used in this paper like Morton's by M Pfister (2014) [21] Eötvös [22] by Viana (2003) and Reynold's, which have been proven to correlate strongly with the studied properties as bubble velocity and aspect ratio, that are analysed in this paper.

1.5 Current state of art in Metal Foam Applications

The motive for using metal foam is coming from nature, it was observed how light a structure could be while maintain a good portion of strength, honeycomb panels are a good example in which it's used in manufacturing of galleys and other aircraft interiors, inspired by the honeycomb structure of beehives, more inspirations from natural materials is bone, sponge or wood,

that leads to many scientific attempts to improve the quality of metal man-made foams, making it industry-worthy; making it cost effective and of acceptable quality through mass production.

Metal foam makes sense in regards to cost when several properties align to be needed in the product, a good product to be produced by metal foam would be lightweight, with high crash energy absorption properties and with good stiffness, which makes it a good application in automotive, aerospace and railway industries

Currently metallic foams are industry-fit in limited number of applications but used experimentally and in trials for many more applications, a good example for an industry-fit application is the company Alulight (ranshofen, Austria) holds a production for Aluminum foam used in door sills, which was used for the Audi Q7 SUV vehicle as a crash absorber, producing 120,000 parts per year and considered the largest serial production of metallic foams in the automotive industry [23]

One of the novel applications of Metal foam is the improving of PCM (phase changing material properties) heat transfer properties. Phase changing materials are becoming a point of interest for researchers due to their ability of storing heat in means of latent heat of fusion, instead of typical sensible heat. Given the high amount of losses occurring due to sensible heat. PCMs are being employed in many applications for energy storage like in construction in which the walls could store heat from morning to warm up the space during the night [24]

Many ways were researched in order to improve thermal conductivity of PCM materials, including conventional ways for aiding the heat transfer through adding fins to the geometry, which is the current most common solution to the low thermal conductivity issue because of the simplicity and the cost of such solution, study [25] concluded that increasing the number of fins or the width of the fins would increase the conductivity of PCM material. Another way to improve the thermal conductivity for PCM is to use honeycomb structure, in

one study where an Aluminum honeycomb structure was created and filled with phase changing material, it was noticed that the heat was spread within the honeycomb material more uniformly, increasing the heat conductivity of PCM material [26], this application is used in Solar energy storage applications. Metal foam has been gaining popularity in PCM applications in aiding with the heat transfer, one study studied the effect of the pore size on the energy absorption of the PCM, and concluded that usage of metal foam aids in the thermal conductivity of the PCM, different pore size effects were concluded in Figure 6 Variation of total time required for complete melting of PCM. The figure compares different porosity percentages, porosity is defined as ration between volume of void space to the volume of solid, and r is average radius of the pores

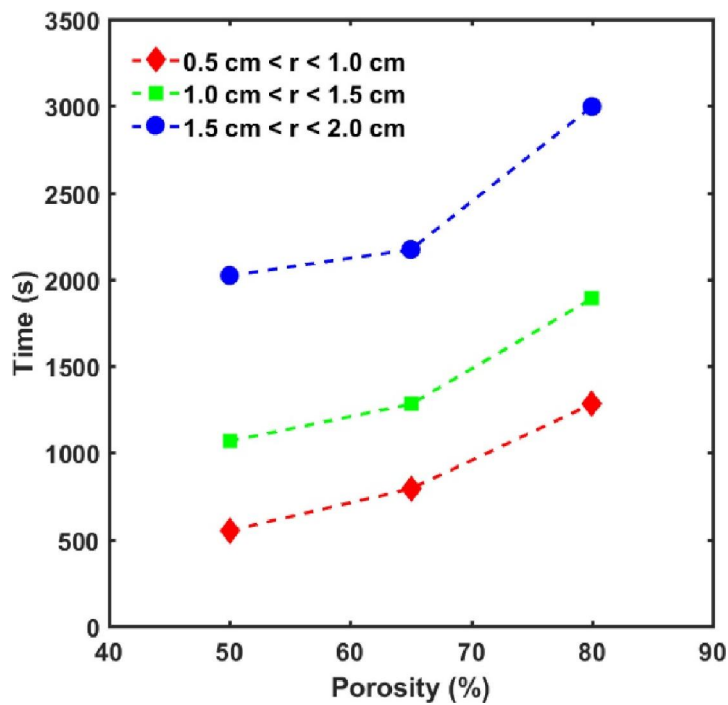


Figure 6 Variation of total time required for complete melting of PCM.

The potential of metal foam can be increased when implemented between 2 metal or composite sheets in what could be called as Aluminum foam sandwich (AFS), such panels are used in many industries, this is very similar to the idea of Nomex, a honeycomb core is a lightweight, strong, non-metallic product manufactured with aramid paper impregnated with a heat resistant phenolic resin, same concept could be applied to metal foam, yet the biggest challenge of using metal foam in such application remains the weight, as for the density for Nomex is attractive parameter for usage in inner body of aircrafts (29 kg/m^3) [27] on average the relative density of manufactured aluminum foam is 10% of the density of the metal (2700 kg/m^3) [28] making

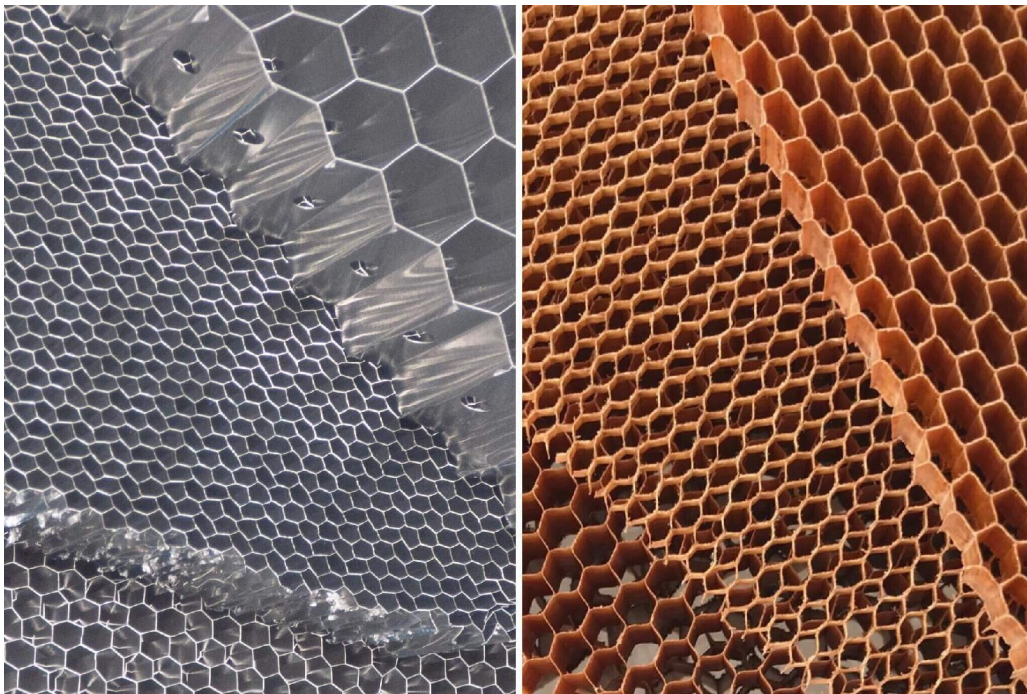


Figure 7 Aluminum honeycomb (left) vs Nomex (Right) [29]

a manufactured metal foam sandwich panel density almost 10 times that of Nomex, while it can retain way higher loads than it's aramid paper counterpart it's still not practical to add such weight for aircrafts, which makes metal foam a better candidate for the aircraft body itself rather than the interiors and galleys of the aircraft, and due to the criticality of this aircraft component it has to go through a long period of research and development before it's green

lit for big scale production, especially when there's strong competition from materials like carbon fiber and composite reinforced polymers.

Nomex is also a better material for heat and electrical insulation, making it more safe in the interior of aircrafts since the cabin should be insulated from the outside due to temperature, and having it not conductive of electricity would help, on the other hand Nomex being made from paper based material, there's high chance it would absorb moisture and even grow fungus if not sealed properly, a look at available commercial options it was found that aluminum honeycomb could be found with densities as low as 50, still double what is offered by the Aramid paper fiber, but it still offers more 3 times the strength under compression loads

Table 1 comparison between Al and fiber honeycomb provided by Plascore. [29] [30]

| | Aerospace Grade | |
|----------------------------|----------------------------------|----------------------------|
| | PAMG-XR1 5052 Aluminum Honeycomb | PN2 Aramid Fiber Honeycomb |
| cell size (mm) | 3.2 | 3.2 |
| density (kg/m3) | 50 | 29 |
| Compression Strength (MPa) | 2.14 | 0.7 |

1.6 Examples of available Metal Foam production equipment

1.6.1 Foaming of metals by direct gas injection (Hydro/Alcan):

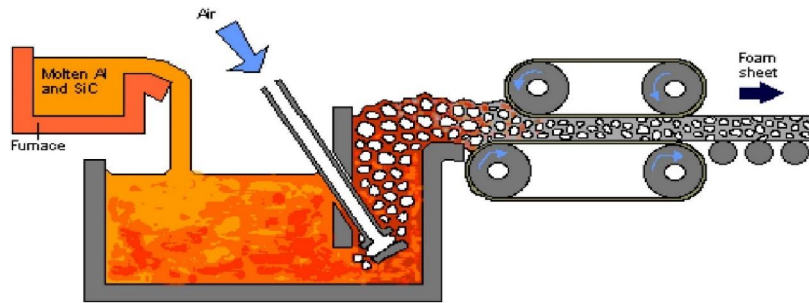


Figure 8 Melt gas injection method [91]

The most common and simple method is to directly inject the gas into the melt, a feasible way to do it was patented in 1991 [31] and currently used by the ALCAN International Ltd., Canada. At present, CYMAT Aluminum Corporation, Canada patented in 1993 [32] in which they introduced the concept of adding particles of MgO to liquid matrix above the metal's liquidus temperature and disperse them by means of an impeller.

In Figure 8 the process of metal foaming by direct injection is shown, The aluminum melt matrix is made by adding additives to reach a viscosity value within an acceptable range, then using a certain nozzle injector system, in which an impeller could be used an inert gas is injected into the molten metal, in which bubbles rise to the top and stabilize under influence of surface tension of the molten metal.

The aluminium melt matrix is made by adding additives to reach a viscosity value within an acceptable range, then using a certain nozzle injector system, in which an impeller could be used an inert gas is injected into the molten metal, in which bubbles rise to the top and stabilize under influence of surface tension of the molten metal.

This study would mainly focus on the direct gas injection method for metal foaming, as it has similarities in the test rig set up that has an injector that injects gas into a liquid. A number of challenges to be faced is the fact that molten aluminium and water have different values of viscosity on below-surface level which would influence the shape of the bubble before it reaches the surface, however this study will examine the common areas between the 2 materials in which the values of viscosity could be similar.

The foam is made by gas injection method, where a rotating impeller or a

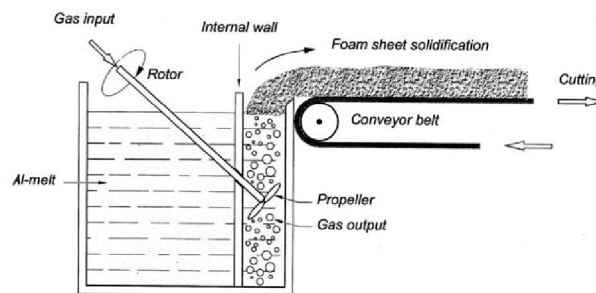


Figure 9 Metal Foam by direct injection

nozzle is used to inject gas into molten aluminum melt, the generated bubble float to the surface of the melt and at this stage after the temperature has cooled down, the stabilized liquid foam is taken to the next stage, which is a mold this mold is temperature regulated in order to maintain the stabilization of the metal foam.

In such process several factors need to be kept monitored: temperature, gas pressure and gas flow rate, the bubble shapes is highly dependent of the shape of the gas nozzle, higher traveling distance taken by the bubble usually lead to more stable foam

Not only both mechanical and physical properties of aluminum foam are affected but composition but also the structure of the cells, when the injected air causes the air bubbles to rise to the surface of the melt forming a liquid foam which is stabilized by means of the ceramic particles on the interface between the gas and the liquid, the impeller design and speed also highly influence of the cell size as well as the wall size.

Stable foam does not occur unless the concentration reached for both SiC and Al₂O₃ is achieved and increasing that concentration also leads to unstable foam. Cell size of the foam would increase with adding SiC and Al₂O₃ to the molten aluminum given the temperature remains constant. Cell wall thickness increases with increasing SiC and Al₂O₃ concentration yet decreases with increasing the Temperature, increasing the gas flow rate and the temperature cause an increase in the cell wall thickness and the cell size. [33]

It was noticed that using different gases gave different outcomes, for example nitrogen cause a higher probability of the bubbles bursts at the surface of the metal. [34]

In a study the authors discussed the foamability of different aluminium-alloy based composites, 15 different aluminium composites were melted and using air injection all the 15 composites were foamed in which foamability was analyzed, and from such values a stability diagram was made, since foamability is dependent on the solid particles in the metal foam, it was possible to sketch dependability of foamability on the presence of solid particles, this was achieved via X-ray Radioscopy. [35]

1.6.1.1 Role of ceramic particles in stabilization of foam:

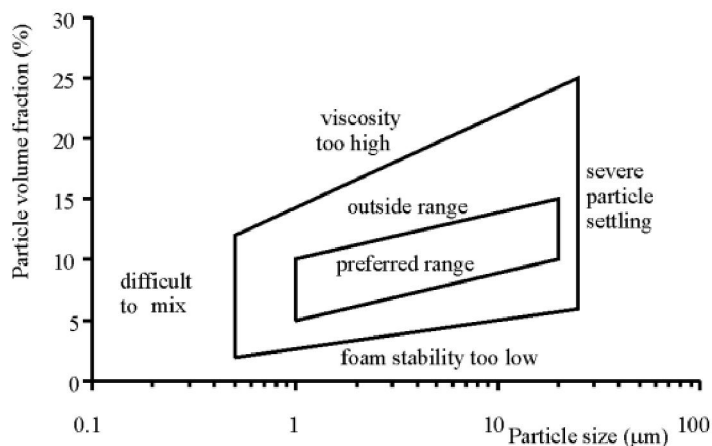


Figure 10 Particle volume fraction, Size for foaming [36]

An impeller is used to disperse the injected gas bubbles in the liquid metal matrix, the addition of ceramic particles enhances the viscosity to aid that propagation also will increase the strength of the cell walls of the solidified metal foam, typically SiC, Al_2O_3 or MgO are used [37], as shown in Figure 10a particle size smaller than 1 μm becomes hard to mix into forming the melt matrix, on the other hand a particle size more than 20 μm could lead to particle sedimentation or settling, increasing the particle volume fraction would lead to a very high viscosity making it hard to disperse the gas bubbles in the melt matrix, this technique has been used to produce metal foam from Al and its alloys with porosity ranging from 80-95% with 3 – 25 mm cell size [36]

Distributing non-metallic particles in a molten metal was discovered to be essential for metal foam stabilization. [38] Adding such particles is known to decrease the merging of 2 foam bubbles to make a bigger bubble, known as coalescence, the phenomenon of coalescence has been discussed by a lot of studies and till now it is a topic of controversy. [39] [40]

1.6.2 Metal foam production by gas agents

Alternative to direct gas injection for the creation of this type of foam a gas is produced by adding of a compound that emit gas after decomposing, every gas agent will require the melt to reach a certain temperature in order to decompose and emit the gas Table 2 could be used as a reference for some of such reactions, the blowing agent is added to the metal foam at 680 C, for titanium hydride usually 1.6% by weight [41] is added to the metal melt, because of the reaction the mixture expands gradually and it usually takes around 15 minutes for the reaction to fully finish, this method is favored because there's no need for an impeller or a gas injector. Different gas agents with their decomposition temperature are shown in table

Table 2 Gas agents for metal foam production

| Agent | Equation | Decompose temperature |
|----------|--|-----------------------|
| TiH_2 | $TiH_2 \rightarrow Ti + H_2$ | 480 °C [42] |
| MnO_2 | $nH_2O + mM \rightarrow M_mO_n + 2 nH$ | [43] |
| $CaCO_2$ | $CaCO_2 \rightarrow CaO + CO_2$ | 830 °C [44] |

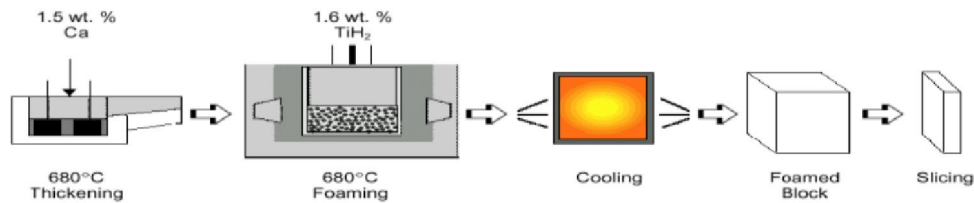


Figure 11 foam by gas agents

One of the big challenges for production of metal foam by means of internal gas release is the collapse of bubbles formed in the melt, means of foam stabilization is usually needed, and while it seems there could be a correlation between the type of alloy used and the minimum wall thinness, one study concluded that the rate of cell wall thinning induced by gas release from the foaming agent has a big effect on the melt –formed bubbles and its collapse during the metal foam process, and the adding of ceramic particle in an attempt of stabilization may be ineffective in reducing the collapse of cells depending on the relation between surface tension of ceramic particle and the melt, the thinning of the cell wall was depicted through [45]

1.6.3 Metal Foam by Mold Casting

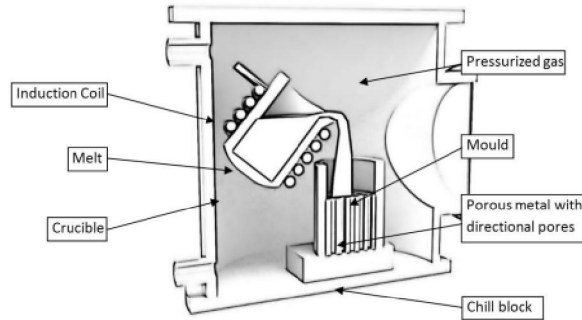


Figure 12 Metal foam by casting [46]

Gas pores are evolved by a metal melt insoluble gas, the pores generated due to the solubility difference between hydrogen in liquid Aluminum and solid aluminum, that makes gas agents are not needed, directional solidification is used to create the pores in the metal from one side to the other, and for this procedure a chiller could be used, the pore size could be influenced by controlling the pressure of the casting chamber, the pores usually have a cylindrical elongated shape, the difference due to phase dependent solubility could be observed in Figure 13

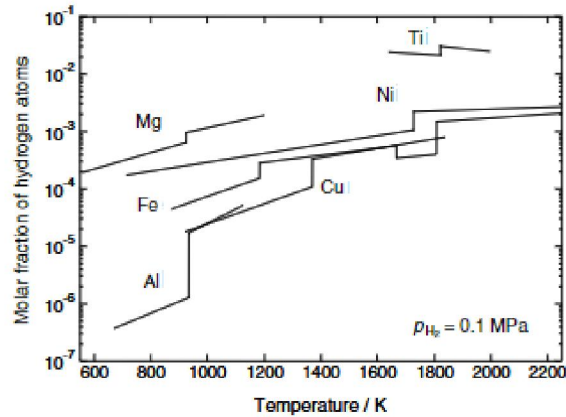


Figure 13 hydrogen solubility based on temperature [47]

1.6.4 Metal Foam production investment casting

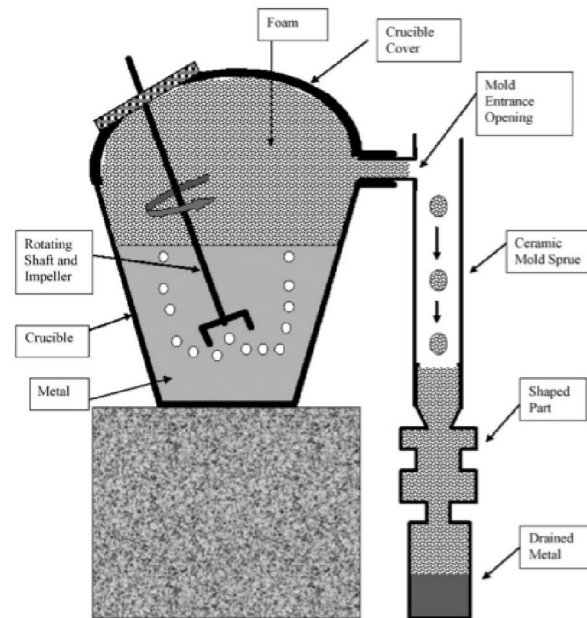


Figure 14 foam production equipment

One device was proposed researchers at the Helsinki University of Technology [48] based on the idea of investment casting, in which a starting material of Aluminium composite with 20% silicon carbide particles were melted in a crucible, then a stainless steel impeller that's connected to a shaft is used to mix the molten metal at 600 to 800 rpm, with an airflow rate of 6 to 7 l/min was maintained at 2 bar. With a melt desired temperature of 690 °C, the foam produced didn't have a uniform pore size, it is only possible to produce very simple shaped and there is no control over the process, yet the process of manufacturing didn't need complicated or expensive tools.

1.6.5 Challenges and opportunities

While the research and development of metal foam has been going for almost half a century [49] researchers are still speculative about many phenomenos that influence the process of foaming, for example it is not clear why a certain amount of stabilizing particles are required to maintain the cell walls intact, also the process of forming pores in the molten metal is usually too complex to be

able to control, most of the knowledge is still empirical and governed by trial and error, and still the industry didn't generate the demand due to several reasons noticed;

1. Metal foam properties aren't good enough given the cost put into producing it
2. Parameters to control metal foam are still up to speculation, pore size or cell wall size is still not fully understood in many foam production processes.
3. Finding a correlation between the bubble size under the surface of the liquid and the foamed bubble above the surface is still under research, and requires expensive and hazardous equipment, for example x-ray to be able to examine the shapes of air bubbles under the surface of liquid metal

1.6.6 Metal foam by compression

In another way to produce aluminum foam, one study used scrap Aluminum Alloy EN AW 2021 waste chips and mixed them with different placeholders, like Himalayan salt, urea and table salt with average particle size of: 5.2, 1.48 and 4,7 mm respectively, a vibrating mechanism was used to disperse the particles as uniformly as possible within the aluminum chips. Later on the specimen was set into a hydraulic press and compressed with a force of 500 kN to be molded in a cylindrical shaped sample with a diameter of 38 mm, 6 samples were prepared in that experiment and stress strain curves were obtained to describe the resulted samples, this way of laboratory created samples is favorable because no heating is required to generate the metal foam, in comparison with most commercially available methods it requires working with aluminum at very high temperatures which makes it usually a hazard when working,

Table 3 comparison between AL foam samples [50]

| Sample number | Space holder | Mass percentage of space holder (%) | total mass after compression (g) | Relative Density |
|---------------|----------------|-------------------------------------|----------------------------------|------------------|
| 1a | Himalayan Salt | 60 | 58 | 0.45 |
| 1b | Himalayan Salt | 60 | 54 | 0.45 |
| 2a | Urea particles | 60 | 53 | 0.4 |
| 2b | Urea particles | 60 | 53 | 0.4 |
| 3a | table salt | 60 | 53 | 0.45 |
| 3b | table salt | 60 | 55 | 0.46 |

Table 4 stress values of samples [50]

| Sample number | yield stress (MPa) | Compressive strength (MPa) at strain 0.6 |
|---------------|--------------------|--|
| 1a | 1.6 | 13.2 |
| 1b | 5.7 | 27.7 |
| 2a | 3.4 | 30.8 |
| 2b | 3.6 | 17.3 |
| 3a | 3.5 | 19.6 |
| 3b | 2.4 | 20.2 |

it could be noted from Table 3 that all samples had 60% mass of the used particle space holder, and in all cases the relative density is around half, i.e. the density of the created foam is half the density of the used alloy. On the other hand when the different samples were tested for yield stress according to a stress strain curve, different samples showed different values of yield stress and compressive strength could be observed in Table 4 [50]

2 Experiment Set-up

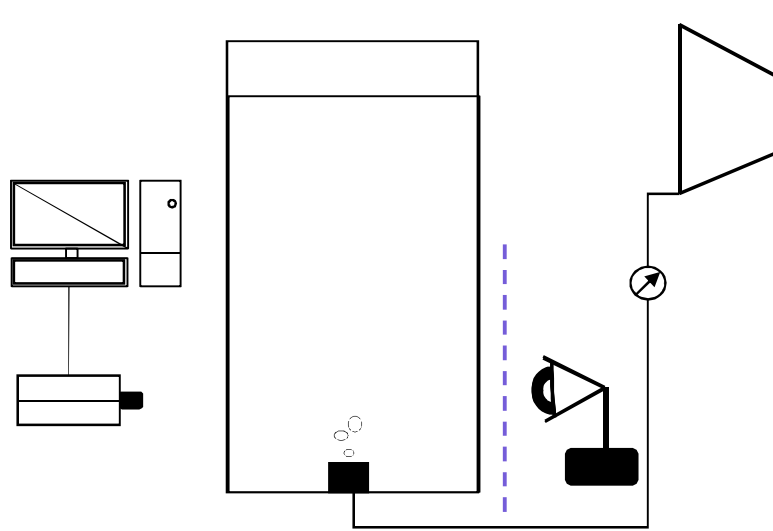


Figure 15 Experiment setup

From the illustrated Figure 15, a glass water tank of dimensions 30 x 20 x 20 cms, glass thickness is 3 mm, filled with liquid. An air compressor is connected by tubes inside the water flow could be adjusted anywhere between 15 to 200 l/h. The flow rate is observed using the flow meter and by connecting the speed camera to a computer. Images of the frequency of 130 Frames per second are sufficient to see how the shape of air bubble will evolve., There are mainly 2 modes of airflow from the air pump, one of which is of a low flow rate (15 l/h) and in that phase, it is noticed that air bubble do not merge during the ascend to the surface of the tank. On the other hand for the second mode, the flow 130 l/h and in this case it is observed air bubble

merging into bigger bubbles, velocity is hard so for the goal of foaming the liquid, a low flow rate is more important to be studied clearly.



- | | |
|------------------------|-------------------|
| 1. High speed camera | 4. Flow meter |
| 2. Nozzle (3D Printed) | 5. Air compressor |
| 3. Light source | 6. Light diffuser |
| 7. tank with liquid | |

Figure 16 photo from lab

As part of this study, a surface tension and viscosity decrease with increase of temperature as stated by Yilmaz (2011) [51], in case of using water it was at 24 °C. In the case of using Ethanol-water mixture in order to study effect on viscosity on the shape of gas bubble by A. Nikumbi (2013) [52] in which an exothermic reaction was observed, the speed camera acquisitions were made at a temperature of 25 °C.

For the usage of speed camera at high number of frame per second (130-180FPS) it was required to have a higher than ambient light intensity, and this was achieved by using a LED light source with several diodes with varying light intensity, and a piece of parchment paper was used as a light diffuser, without the light diffuser the images had a high image-contrast difference which made calibrating the pixel to length value hard, since one area where the light was focused was bright, while the rest of the tank remained too dark to analyse, the use of a light diffuser made the image obtained by the speed

camera more homogenous when comparing dark pixels to light pixels and gave more accurate results.

3 Methodology

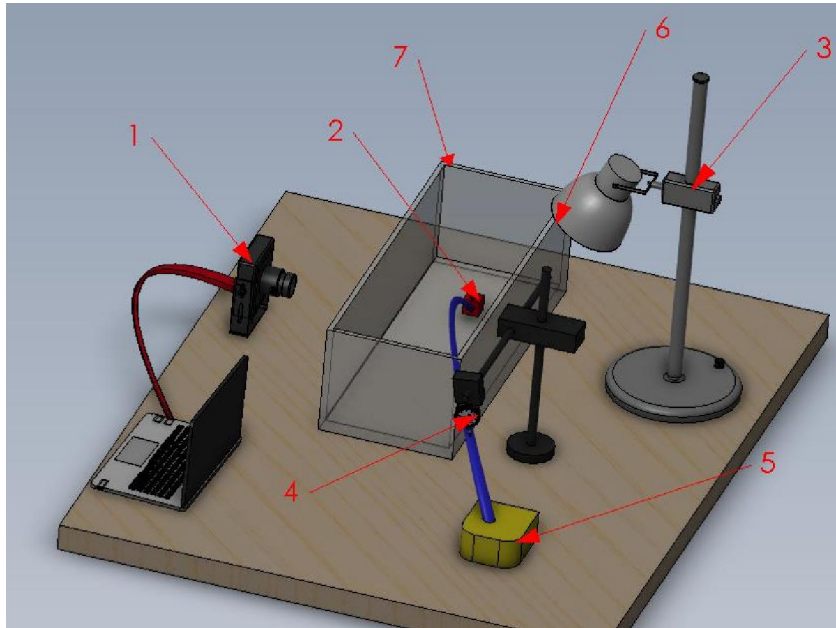


Figure 17 Equipment used

- | | |
|------------------------|-------------------|
| 1. High speed camera | 4. Flow meter |
| 2. Nozzle (3D Printed) | 5. Air compressor |
| 3. Light source | 6. Light diffuser |
| 7. tank with liquid | |

3.1 Idea of a foaming model

Due to the complex nature of predicting the behaviour in the process of foam formation, a foaming model was proposed based on water and alcohol, such models were used in other studies like the study on bubble size in polyvinyl alcohol (PVA) solution, in which parameters such as average bubble size and volume flow rate aided in the prediction of required parameters for the metal foam. Study proved a good match between the PVA experiment model and the carried out numerical simulation [53]

In this study a Foam Model is based on ethanol and water, in which ethanol is added to water to act as a surfactant that decreases the value of surface tension and viscosity and hence generating foam by means of trapping the air under the surface of the liquid.

3.1.1 Comparison between the Foam Model and Aluminium Model:

3.1.1.1 Viscosity of Aluminium

Many studies were concerned with the study of viscosity of liquid Aluminium, due to the complexity of measuring the viscosity of a liquid metal at a temperature about 700 Celsius, many theoretical models are proposed with varying degrees of accuracy, currently it is concluded that main factor of the value of viscosity of Aluminium is its purity [54], with a value of viscosity between 1.0–1.4 mPa·s at the melting point, also for binary mixtures adding Si the viscosity drops, making silicon a good option for the production of Al foam, while Ti; Ni; Cu; Cr; Mn; causes an increase in viscosity

For foaming to happen, a gas is directly injected into a metallic melt then by means of an impeller the bubbles are distributed uniformly through the melt, air flow is usually kept at 30 to 60 l/h, with a pressure of 0.2MPa and foaming temperature is usually 660 – 680 Celsius.

It was shown that increasing volume of added SiC would increase cell size of stabilized AL foam, while also increasing the particle size of SiC would increase the cell size as well. With similar correlation when compared additives particle size and wall thickness, when used additive particle size is increased the cell wall thickness is increased. It was also shown that increasing the foam temperature decreased the cell wall thickness of produced foam. [55]

3.2 Image acquisition equipment

A speed camera with a separate light source has been used, different acquisitions were taken for different FPS, the camera could take as many as

1200FPS, yet 130FPS to 180FPS were enough to trace different shapes of gas bubbles.

The camera was connected to a computer and using provided software it was possible to have a slow-motion video of the gas bubble, the exposure, FPS, sample time could be changed through the camera software, while the focus has to be adjusted manually through an externally attached lens.

It is noted that the high intensity light source was required for the experiment, the higher the FPS value the higher intensity was required through the light source [21].

3.3 Viscosity Meter



Figure 18 Viscosity measuring equipment

Vibro viscosity meter available in the TUL lab, is able to provide a continuous signal of measurement of the current value of viscosity and temperature, since the temperature affects the viscosity, the sensor plates, with a low frequency of 30 Hz and an amplitude of less than 1 mm, apply very little load to the sample. So, the viscometer can continuously obtain stable viscosity values without causing a temperature rise or

damaging the sample. The viscometer uses the Tuning-fork Vibration Method. So, use much care was taken to avoid external vibration, especially when measuring low viscosity. The device helped with creating independent results and to adjust liquid properties of the mixture to correspond to required values to perform the experiment. Lab measured values could be observed in the below graph, another study is presented for validation, both studies are a good match. [56]



Figure 19 Viscosity measuring equipment at TUL

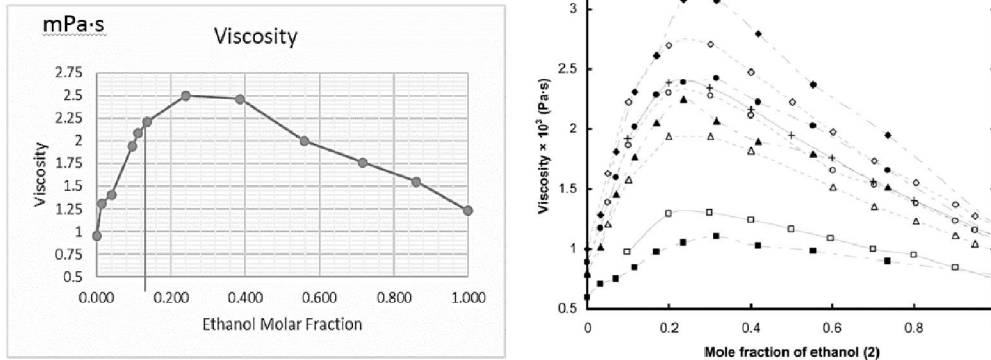


Figure 20 lab measured viscosity (left), journal validated results [57] (right)

3.4 Surface Tension Meter (Bubble pressure tension-meter):



Figure 21 measuring Surface tension

The tension-meter is available at the TUL lab is able to measure surface tension based on the bubble pressure method which is commonly used to measure the dynamic surface tension for liquids containing surfactants or other impurities, the measuring device usually blow air bubbles at a constant rate through a thin tube that is submerged in the liquid, the pressure keeps increasing till it reaches the maximum value and detach off the capillary tube. The device helped with creating independent results and to adjust liquid properties of the mixture to correspond to required values to perform the experiment. Lab measured values could be observed in the below graph Figure 22, another study is presented for validation, both studies are a good match. [56]

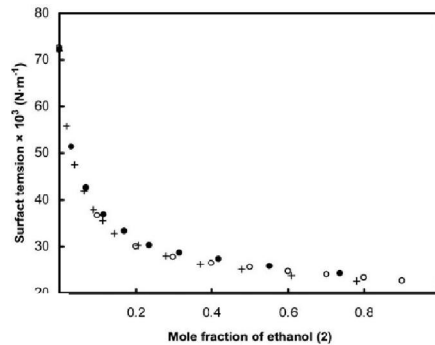
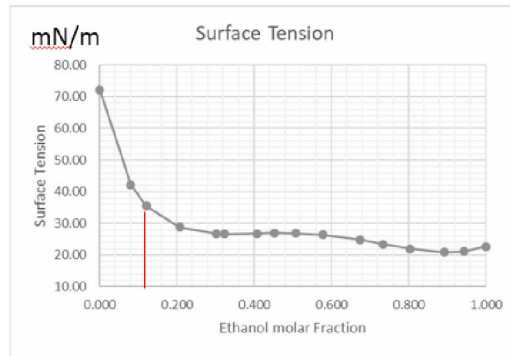


Figure 22 Lab measured results (Top) independent journal results, of 3 different experiments each indicated by its own symbol [55] (Bottom)

3.5 Image processing software

Digital image processing has provided many ways to be able to efficiently analyse the results of foam, or monitor the change of the bubble under the surface of water. Usually images captured by a camera are needed to be converted to an 8 bit format, by the usage of a method of thresholding which is method of segmentation, is a way to further partition a continuous gradient picture into different segments / sections, the result of a segmented image is usually a photo with separate mono-coloured parts, mainly the goal of segmenting is to find the edges of certain objects of the image segmented images are widely used in computer vision.

A quantitative way to analyse foam could be by the usage of digital image processing, usually an algorithm is used to calculate the circularity of contours

in the binary image, the circularity is calculated by achieve this, a common measure of circularity is given by four times pi times the area divided by the perimeter squared:

$$C = \frac{4 \pi A}{P^2} \quad (5.1)$$

Where C is the circularity, A is the area and P is the perimeter. For a circle such value could be between 0 and 1, and using DIP software it possible to detect number of bubbles, average area of each bubble, and a distribution of the radii, which will be demonstrated later in the results parts of this body of work, such technique was used to characterize foam where the bubble size was correlated to the foam rheology [58]

Also aluminium foam was analysed for uniformity by the usage of DIP in which sections of the foam were taken in which they were well-lit, transformed into grey binary images and analysed and the method showed an difference of 4% between planar porosity calculated and volume porosity measured [59], foam stability is also another parameter with attempts to quantify, several industries are interested in such parameters from diary industries to petroleum, especially with the addition of surfactant to monitor the effect of changing the values of surface tension and viscosity to affect the production of foam. In one study it was possible to analyse the stability of foam by taking a picture every 10 seconds and by means of segmentation it was possible to measure the rate of decay of different types of beer, a correlation with a surface tension concluded that lower values of surface tension is an important factor for foam formation [60]

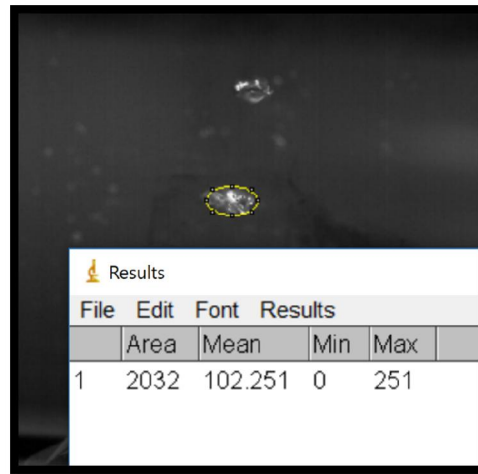


Figure 23 Image processing software

In order to calculate bubble size, velocity and distance travelled it was required to use image processing software, which can process RAW format images. Open-source, Java based software was used, in which it is required to define a horizontal and vertical Pixel to unit ratio, in which the software can measure a number of pixels, and if those pixels form a shape of a known length, then it possible to measure the size of any object on the image, given reference object and measured object are at equal distances from the camera lens. This method was used for calculating diameter, and distance travelled by the bubble from the nozzle, by obtaining the time of the image frame from the camera it is possible to calculate the velocity of the air bubble, also the acceleration, and those results were incorporated into calculating dimensionless numbers used for describing the shape of the bubble later on in this paper.

3.6 Flow meter

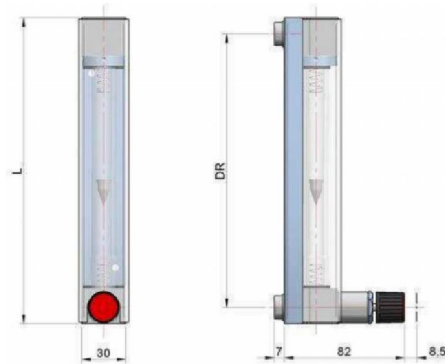


Figure 24 Flow meter (manufacturer Manual)

An airflow meter was mounted in between the air pump the tank, it was taken into consideration that the flow meter needed to be perfectly vertical as any inclination cause an increase in the reading error.

The flow meter chosen was based on the variable area principle, which is obtained by a float that moves inside a borosilicate glass tapered tube, the fluid moves up (against gravity) with enough space for flow, equilibrium is achieved through an equilibrium of forces.

The flow meter comes with a build-in flow regulator, which had a lower range of flow control than that of the air compressor.

Table 5- Flow meter properties (Values provided from product catalogue by supplier)

| | |
|-----------------------------|------------------|
| Accuracy | 3% |
| Operating Fluid Temperature | -20 °C to +80 °C |
| Ambient Temperature | -20 °C to +80 °C |
| Flow range | 15 - 180 l/h |

3.7 Air compressor

A variable flow air compressor was used, the range could be adjusted through a dial switch, the compressor could provide up to 350 l/h of air, and this dial was used to moderate higher range of flow, while the flow meter dial was used to refine the value to a more specific range.

With the help of 3D printing, it was possible to model through CAD software, to manufacture different sizes of air nozzles, varying from 1 mm to 5 mm diameter, to aid in the study of the effect of nozzle diameter on the gas bubble shape, study by M. Versluis (2013) [61]. as well as by Aly H [62]

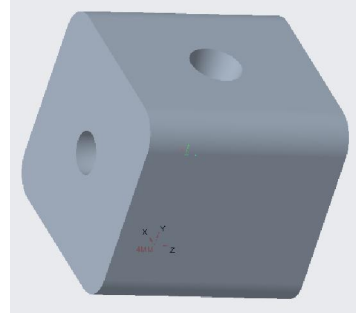


Figure 25 3D printed nozzle

3.8 Dimensionless Parameters

3.8.1 Morton number

$$Mo = \frac{g\mu_c^4\Delta\rho}{\rho_c\sigma^3} \quad (5.2)$$

g is the acceleration of gravity, μ is the viscosity of the surrounding fluid, ρ the density of the surrounding fluid, $\Delta\rho$ the difference in density of the phases and σ is the surface tension coefficient. Morton's number usually is used with Eotvos number to describe the liquid for bubble dynamics, due to the fact that Eotvos number takes the radius of the bubble in consideration, and that's changing continuously there's a need to have another parameter to define the state of the liquid.

Morton number was developed during a dimensionless analysis for an experiment of a bubble rising in a stagnant fluid, and it is based on combination of Weber and Froude numbers.

3.8.2 Eötvös number

$$Eo = \frac{\Delta\rho g L^2}{\sigma} \quad (5.3)$$

$\Delta\rho$: Difference in density of the two phases, g : gravitational acceleration, L : characteristic length, could be considered bubble diameter here and σ : surface tension.

Eötvös number could also be called bond number and it describes the ratio of forces to gravity to surface tension influence in the shape of the bubble.

3.8.3 Reynolds number

$$Re = \frac{\rho u L}{\mu} \quad (5.4)$$

where ρ is the density of the fluid (SI units: kg/m³), u is the velocity of the fluid with respect to the object (m/s), L is a characteristic linear dimension (m), in this case it would be diameter of the bubble and μ is the dynamic viscosity of the fluid (Pa·s or N·s/m² or kg/m·s).

The most common use of Re is determining whether this flow is laminar, transitional or turbulent, Low Reynolds numbers occur when a flow has dominant viscous forces, it's constantly moving, at lower velocities. While Turbulent flows are characterised by high values of Reynolds number (more than 1500) which could mean the flow contains eddies, vortices and other flow turbulences.

In this study the significance of Reynolds number is to measure how turbulent is the flow around the air bubble, and thus it is possible to quantify the influence of the turbulence on the deformation on the bubble shape or its aspect ratio.

4 Results and Discussion

4.1 Water with Nozzle diameter is 3mm and $v = 15$ l/h [D3V15]

Table 6 - showing properties for case of flow rate 15 l/h

| | |
|---|----------------------|
| surface tension [mN/m] | 72 |
| Morton's Number | 1.59527E-11 |
| Kinematic Viscosity [m ² /s] | 105×10^{-8} |
| Sample time [s] | 0.275 |

4.1.1 Bubble shapes

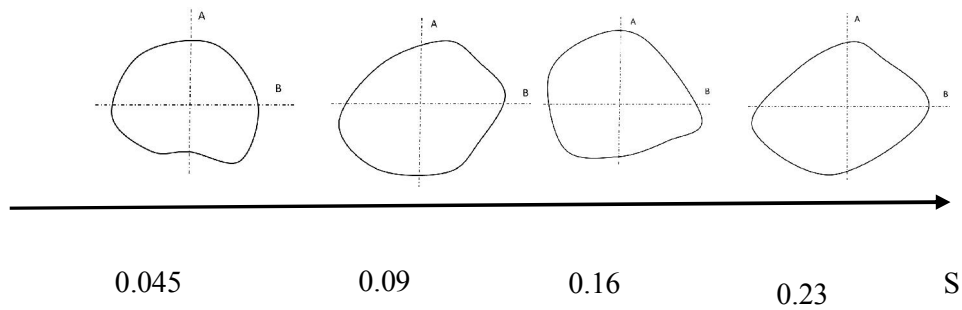


Figure 26 - Bubble shape change w time

Table 7 - properties of corresponding bubbles in Figure 26

| | | | | |
|--------------------------------|---------|---------|---------|---------|
| <i>Time [s.]</i> | 0.045 | 0.09 | 0.16 | 0.235 |
| <i>A [mm]</i> | 6.9 | 8.4 | 9.1 | 7.792 |
| <i>B [mm]</i> | 10 | 11.93 | 10.17 | 8.33 |
| <i>Distance Travelled [mm]</i> | 15.2 | 28.636 | 55.9 | 90.102 |
| <i>Velocity [m/s]</i> | 0.285 | 0.33224 | 0.59333 | 0.47768 |
| <i>aspect ratio</i> | 0.69 | 0.70411 | 0.89479 | 0.93541 |
| <i>Eu</i> | 0.25381 | 0.36963 | 0.34842 | 0.24472 |

Figure 26 - Bubble shape change w time shows bubble shapes for nozzle diameter = 3 mm and Volume flow rate if 15 l/h for this acquisition it was noticed that the bubbles rise uniformly, in a steady state. The bubble would start at the nozzle mouth in the shape of a mushroom head, and as it rises it would take a more spherical shape till mid-distance where some wobbling occur, a significant amount of bubble remained trapped under the liquid surface, and that could point out that the surface tension of water is adequate

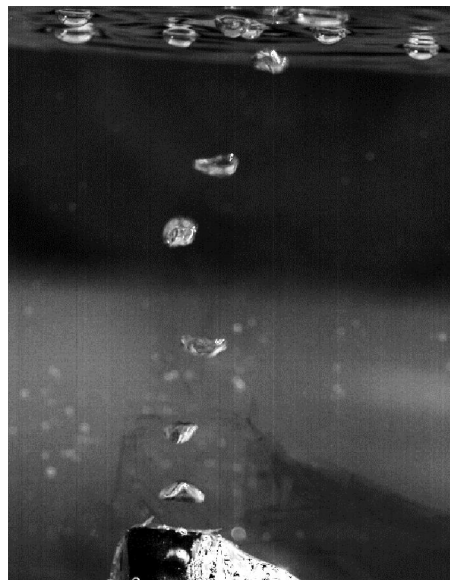


Figure 27- bubbles trapped under water surface

for forming foam with bubbles of properties described, while properties in Figure 28 Corresponds to the bubble shapes in Figure 26

Figure 27 shows image acquired through the speed camera showing for a flow rate of 15 l/h it was possible to trap the air bubbles in the liquid surface.

Aspect ratio is a good way to deduce how uniform is the bubble shape, also several empirical equations have offered equations for the bubble velocity in a relation to the aspect ratio such as study by Baz-Rodriguez (2012) [63]

Figure 29 aspect ratio vs timeshows the change of aspect ratio of the gas bubble versus time. The values at many time instances seem to approach 1, which could make it seem that the bubble is more spherical-like.

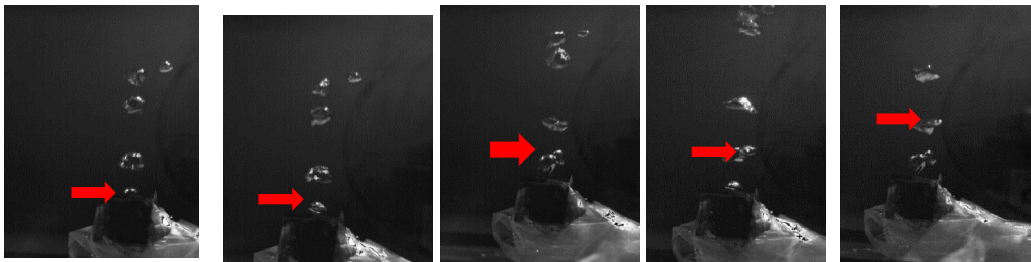


Figure 28 rising bubble sequence

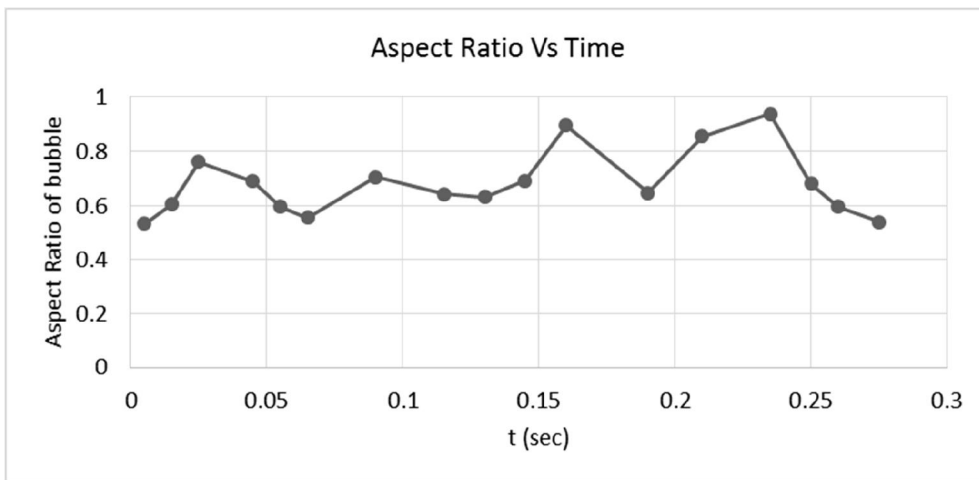


Figure 29 aspect ratio vs time

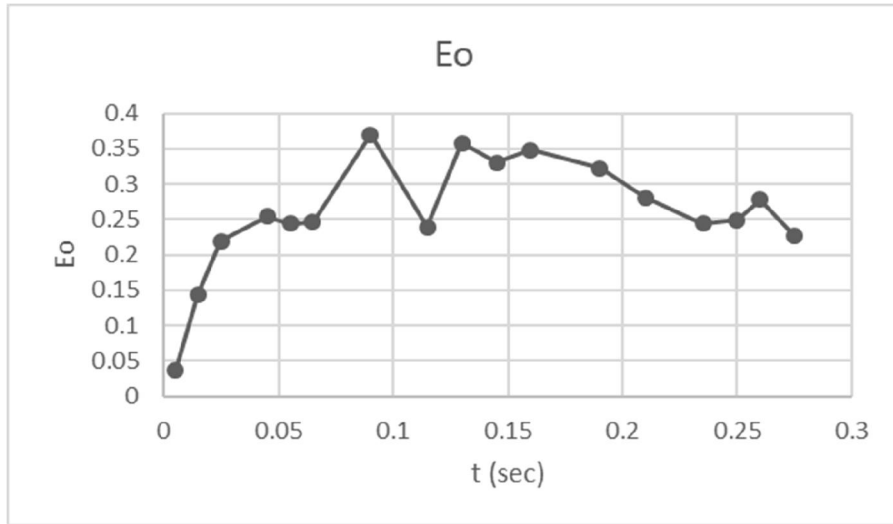


Figure 30-Eotvos values change with time

Eötvös describes the effect of gravitational forces compared to surface tension forces, when observing Figure 30 It shows all values are below 1, thus it could be assumed that surface tension at the liquid-gas boundary of the bubble is highly influencing the resultant shape when compared to gravitational forces

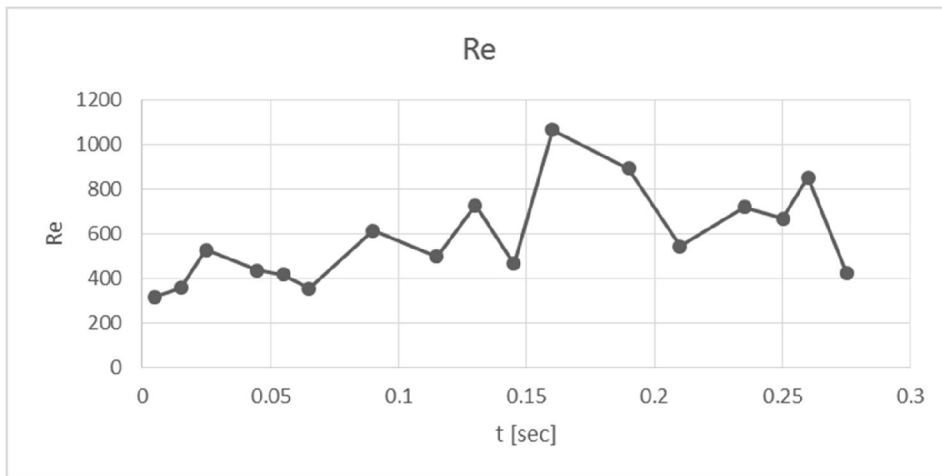


Figure 31 Re vs time for rising bubble

Figure 31 denotes the change of Re number with time values are noticed to be much lower than that of higher flow rate, with the peak in Re ($Re = 1067$, $t = 0.16$ s) coincide with the maximum velocity. Noted from the change in

Aspect Ratio and Re , the flow could be described as mostly laminar and this was better optimum to describe formation of the gas bubble with minor influence from unmonitored factors, such as bubble merging or splitting, drag forces due to high flow by the gas bubble.

4.1.2 Monitoring the effect of a higher flowrate

The experiment was carried out at different parameters, 2 cases are compared where the liquid used is water D5V130 and D3V15, where D5 means nozzle diameter is 5 mm, and V130 corresponds to a volume flow rate of 130 l/hr, below table shows the 2 compared cases

Table 8 comparison between 2 case studies

| | | |
|---|----------|----------|
| Flow rate [l/h] | 15 | 130 |
| Nozzle Diameter [mm] | 3 | 5 |
| Surface tension [mN/m] | 72 | 72 |
| Morton's Number | 1.60E-11 | 1.60E-11 |
| Kinematic Viscosity [m ² /s] | 1.05E-06 | 1.05E-06 |
| Sample time [s] | 0.275 | 0.32 |

4.1 Comparison between D5V130 and D3V15:

Figure 32 shows a comparison for D5V130 (nozzle diameter of 5mm, flowrate of 130 l/h) and D3V15, indicating Reynold's number variance with time. For D5V130, the first peak occurs at $t = 0.12$ is when the bubble reaches maximum diameter before it detaches from the nozzle, notice that the diameter increases

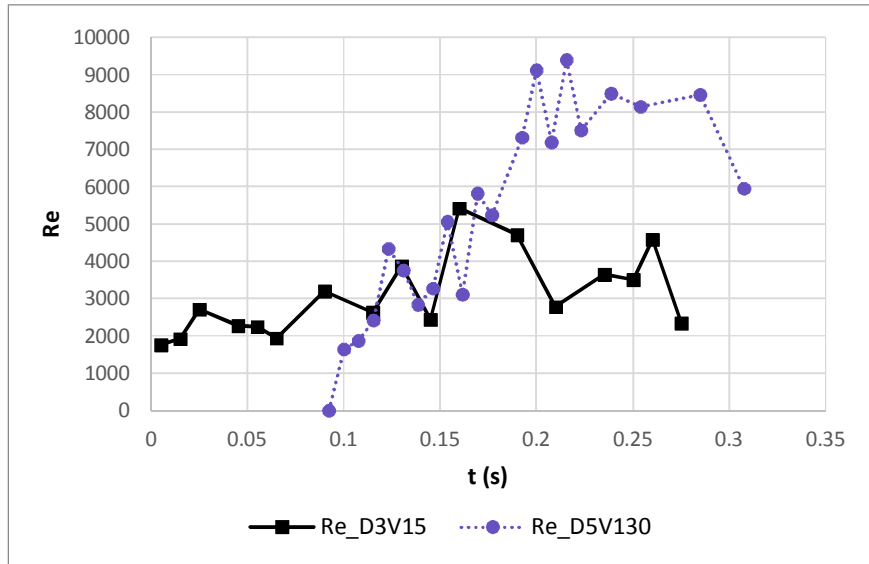


Figure 32 - Reynold's number values of nozzle diameter 3 mm and flowrate 130 l/h compared to D3V15

once more when the second bubble merges into the first, and then it keeps increasing as the bubble rises to the surface. The maximum value of Re is 9418 at $t = 0.215$ s and it could be explained as when the bubble merge occur, turbulence is high as the second bubble is pushing the gas/liquid boundary to influencing the diameter to increase, diameter.

D3V15 values are noticed to be much lower than that of higher flow rate, with the peak in Re ($Re = 1067$, $t = 0.16$ s) coincide with the maximum velocity. Noted from the change in Diameter (figure 4) and Re, the flow could be

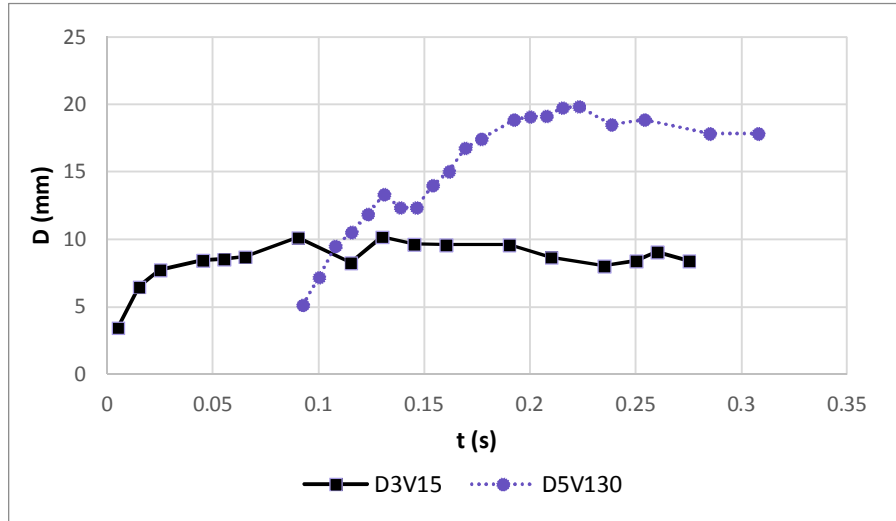


Figure 33 - Diameter values of nozzle diameter 3 mm and flowrate 130 l/h compared to D3V15

described as mostly laminar and this was better optimum to describe formation of the gas bubble with minor influence from unmonitored factors, such as bubble merging or splitting, drag forces due to high flow by the gas bubble. When calculating the characteristic length for Re, the radii of the ellipsoidal were used to calculate volume and area, which were divided to get the characteristic length, which should give a more accurate value.

Figure 4 is a plot of the relation between diameter and time. The diameter was measured as a mean diameter for bubble of an varying radius. The highest rate of increase of radius with respect to time could be noticed when merging happens, after than the instant of biggest radius is very close to the instant of highest Re number which could be contributed to turbulence and expansion of the gas-liquid boundary due to the merging of the 2 bubbles. It is observed that for higher flow rates the diameter is bigger, at a certain time, $t = 0.13$ for D3V15 (Diameter = 3 mm, flowrate = 15 l/h) the diameter has minor fluctuations and could be considered stabilized, but when analysing the radius for the higher flow rate (D5V130) the diameter seem to hardly achieve

stabilization, this could be related to higher turbulence, and merging of air bubbles.

4.1.1 Comparison to similar studies:

A study by Jinsong [64] was concerned with bubble rising in viscous liquid in which a CFD simulation was done and validated by experimental means, the simulation adopted Navier-Stokes equation to simulate the shape of the gas bubble while rising in stagnant liquid at Re values below 200 and bond number values below 200, the simulation tries different samples of liquids and goes on to predict shape of the bubble, diameter then Re and Bo (bond number)






























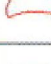



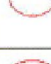





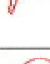

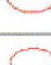







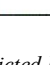
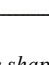

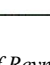
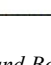


| Parameters | | Bo* | | | | | | | |
|------------|-----|---|---|---|---|---|--|---|---|
| | | 0.5 | 1 | 5 | 10 | 20 | 50 | 100 | 200 |
| Re' | 1 |  |  |  |  |  |  |  |  |
| | 5 |  |  |  |  |  |  |  |  |
| | 10 |  |  |  |  |  |  |  |  |
| | 20 |  |  |  |  |  |  |  |  |
| | 50 |  |  |  |  |  |  |  |  |
| | 100 |  |  |  |  |  |  |  |  |
| | 200 |  |  |  |  |  |  |  |  |

Figure 34 The predicted bubble shapes as a function of Reynolds and Bond numbers [64].

Another study by Gholamreza [65] in which using volume of fluid method to predict the different parameters of a rising bubble in stagnant fluid, also with the aid of the dimensionless parameters: Re, Bo (Eo) and Morton, the study

provided a graph of the change of the aspect ratio of the rising bubble in a stagnant liquid, results were also validated by experimental means

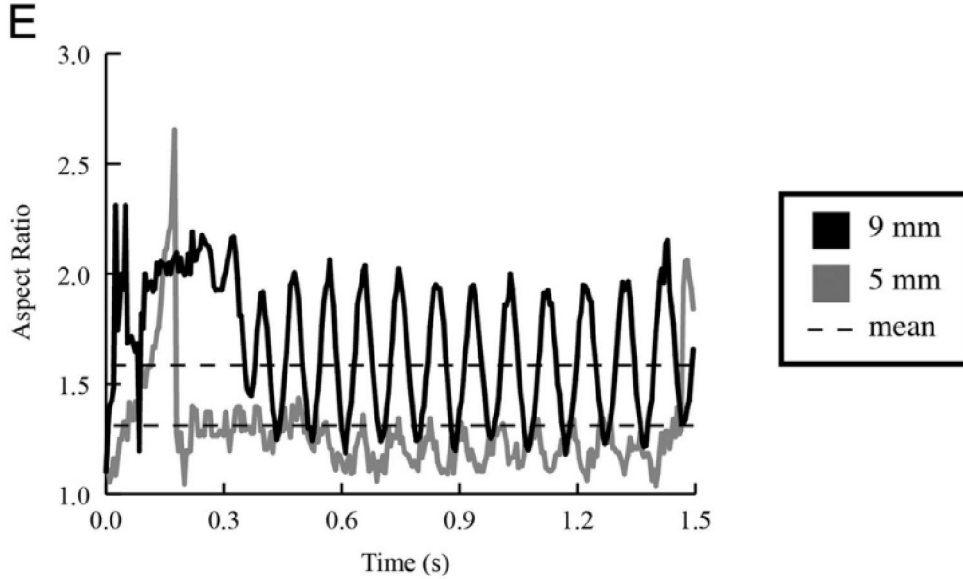


Figure 35 aspect ration change for a bubble rising in stagnat fluid [65]

4.2 Water-Ethanol mixture with the nozzle diameter of 3mm and $v = 15$ l/h

The idea behind adding ethanol to the water is to study the effect of changing the values of viscosity, surface tension and density on the shape of the air bubble and examine the interaction between different gas bubbles, for the reason it was required to measure or calculate those values, there were no equipment ready for this purpose, thus using volumetric ratios provided by previous study by I. S. Khattab (2012) [57] it was possible to postulate those values.

in order to achieve a viscosity of 2×10^{-3} Pa. s, it is required to obtain a molar fraction of ethanol of 0.13, this attained by mixing 8 litres of water (444.1 moles) and 3.875 litres of Ethanol given it's pure (66.359 moles) – the used Ethanol was with 95% purity, that was also taken into consideration.

The Ethanol water Mixture should affect the values of density, surface tension and viscosity, for the mixture the density was taken by 930.5 kg/m³ [57]

It is worth stating that after the ethanol was added to water, the viscosity has increased, yet surface tension of the liquid was decreased. Also mixing water and ethanol would lead to an exothermic reaction which lead to an increase in temperature which was taken into consideration, by the usage of thermometer.

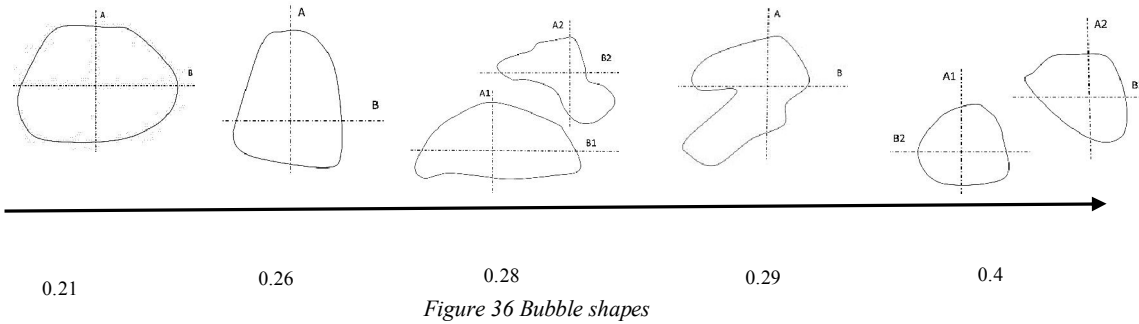


Figure 36 Bubble shapes

Table 9 properties of corresponding bubbles in Figure 36 Bubble shapes

| Time (s) | 0.215 | 0.26 | 0.28 | | 0.295 | 0.4 | |
|---------------------------|-------|--------|----------|----------|-------|----------|----------|
| | | | bubble 1 | bubble 2 | | bubble 1 | bubble 2 |
| A (mm) | 7.2 | 5.56 | 11.5 | 10.4 | 11.1 | 10.1 | 12 |
| B (mm) | 9.14 | 12.2 | 10.1 | 7 | 10.92 | 10 | 8.4 |
| Distance from nozzle (mm) | 11.8 | 23.415 | 30.6 | 32.6 | 35.2 | 70.6 | 76 |
| Velocity (m/s) | 0.213 | 0.276 | 0.11 | 0.6 | 0.31 | 0.28 | 0.5 |
| Aspect Ratio | 0.78 | 0.45 | 1.1 | 1.4 | 1.02 | 1 | 1.4 |
| Eu | 0.53 | 0.49 | 0.94 | 0.57 | 0.99 | 0.82 | 0.82 |

So most of the acquisitions were measured at a room temperature around 25 °C, Surface tension value was taken as 31 mN/m/, given the molar ratio [57]

Figure 36 shows the bubble shapes and properties when the ethanol was added to the water, it was noticed that the bubble formation dynamics have changed, for the same flow rate of just water 15 l/h instead of having each bubble rise on its own to the surface of the fluid, Ethanol-water mixture exhibits a different behaviour which one bubble is shot out of the nozzle then seems to be pulled back till the second bubble emerges, and then what happens later is a merging of these bubble and floating of the 2 bubbles together then another split occurs to 2 bubbles which usually have an aspect ratio close to 1.

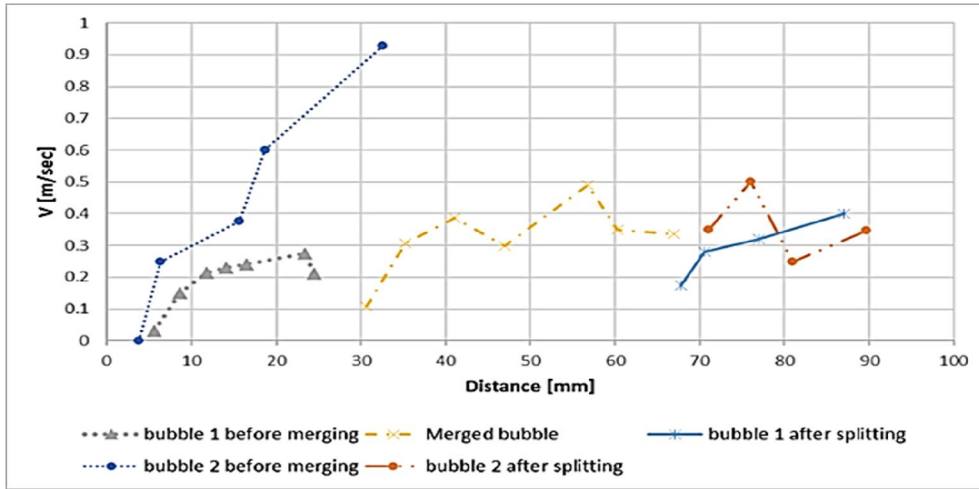


Figure 37: Velocity vs Distance from nozzle

In Figure 36 stages were divided according the merging and splitting of the bubbles, as it was thought that would be the best way to describe this phenomenon, also it would be better to coordinate such stages with the graphs

Figure 37 shows the change of velocity before and after bubble merging versus distance travelled, it is noted that the bubble 1 is the one released from the nozzle first, then bubble 2 is released afterwards. The bubble 1 (triangle marked points) starts to slow down, as bubble 2 (dotted line, circle marker) speeds up, then the 2 bubbles merge at about 30 mm from the nozzle outlet, with an average velocity of 0.4 m/s till splitting occurs at about 70 mm from the nozzle and they reach the surface separately.

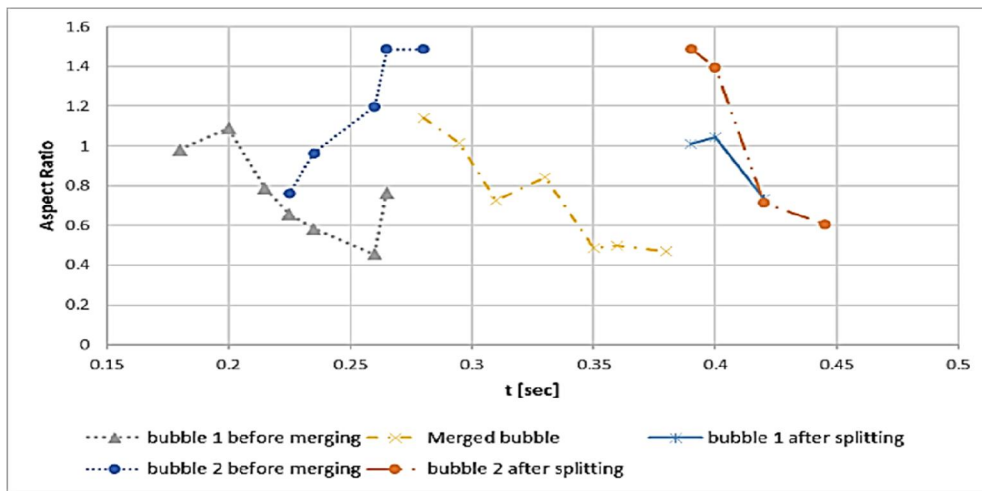


Figure 38 Aspect Ratio vs time

Figure 38 traces the change of aspect ratio of the bubbles with time, bubble 1 starts earlier because released first from the nozzle, it is noticeable that each

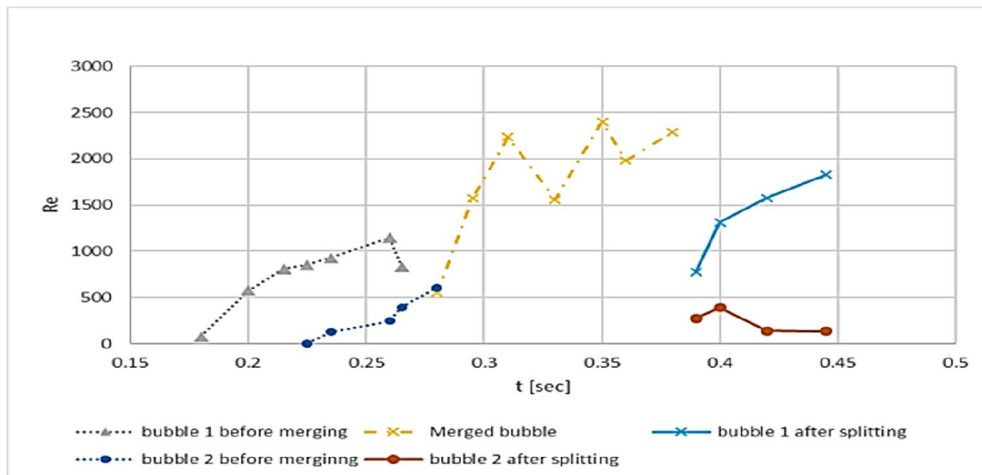


Figure 39 Re vs time

bubble was released with a different aspect ratio, which indicates a sequential effect between the bubbles i.e. the sequence of the bubble affects its shape. Just before merging bubble 1 is more elongated horizontally, while change of Re with time is describe by Figure 39. It is noticed that the area with highest turbulence with Re values ranging between (500 and 2500) is in the merged bubble part, bubbles before and after merging have a generally lower Re number. One of bubbles after splitting seem to have significantly lower Re number as they approach the surface of the water tank.

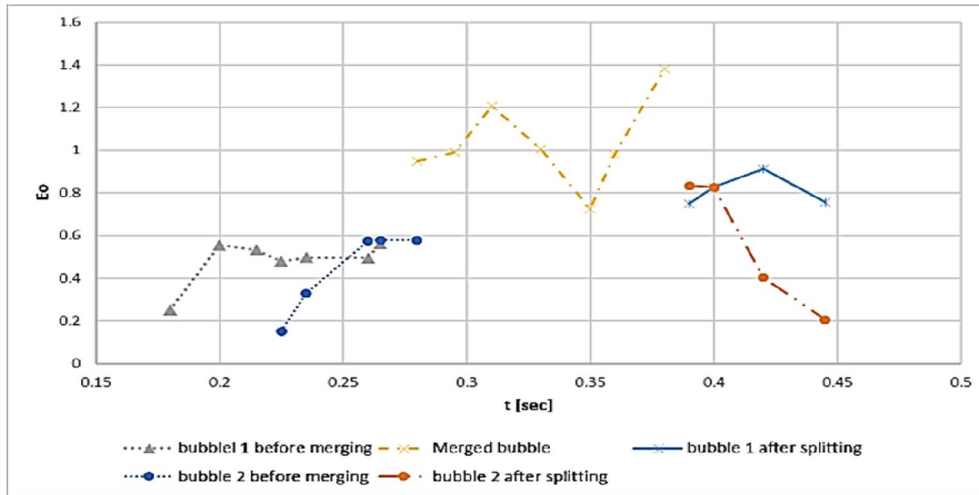


Figure 40 Eötvös vs time

The bubble 2 is more elongated vertically (aspect ratio = 1.5), as the merging occurs the aspect ratio starts at one, then it becomes more oriented towards a longer horizontal length.

Figure 40 is concerned with variations of Eötvös number with time, as the merging of the gas bubble increases the mass, it is obvious that before and after merging surface tension force dominates the shape of the bubble, while at the merged state the gravitational force dominates which could correlate to the increased mass of the air bubble. For bubble 1 before merging values vary between 0.21 and 0.58, then after splitting bubble, it is around 0.7 to 0.9 while that for bubble 2 it is from 0.18 to 0.6, and after splitting it changes from 0.83 to 0.2. For the merged bigger bubble is varies between 0.9 and 1.4.

4.3 Analysis for produced Foam in water Ethanol mixture

In the first part of the experiment it was decided to reach optimum flow rate for bubble foam size, which is believe to correspond to cell size in the case of solidification of liquid. And for such application it was thought it is needed to go in two directions to find the optimum conditions, the main criteria to be measured for the foaming process is first, the Molar fraction of ethanol that could correspond to the viscosity and surface tension change by Silicon particles in the molten Aluminium, lastly the flow rate in which the gas bubble are trapped under the liquid surface as well as the effect of coalescence or bubble merging, which could be relate to the cell size in aluminium manufactured foam. All flow rates were measured at an Ethanol molar fraction of $X_e = 0.13$

4.3.1 Effect of Molar Fraction of Ethanol on the foamability of the mixture:

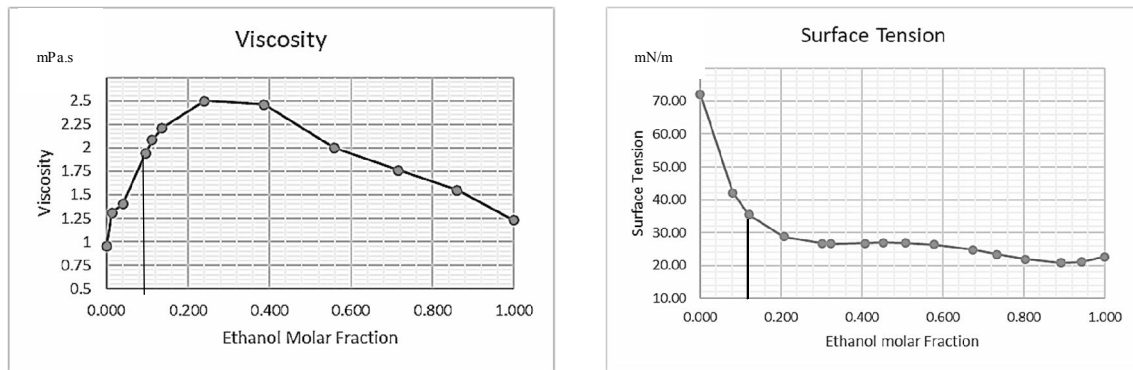


Figure 41: Viscosity vs Ethanol Molar Fraction (left) – Surface tension vs Ethanol Molar fraction (Right)

The molar fraction of ethanol of 0.13, this attained by mixing 8 litres of water (444.1 moles) and 3.875 litres of Ethanol given it's pure (66.359 moles) – The surface tension tested in the lab gave the value of 43.4 mN/m, the mixture density is 995 Kg/m³, and viscosity of 2 mPa.s.

From the above Figure 41, it is shows results obtained in the lab, viscosity doesn't have a linear correlation with the molar fraction of ethanol, and for that reason it was advised to use a molar fraction below 0.2.

While for the surface tension values it was observed a high decline in its value after 0.13 for the molar fraction, and thus the used mixture was kept at a value below 0.13

4.3.2 Flow rate effect on foam size:

in means to decide the best flow rate as it influences the surface foam shape,

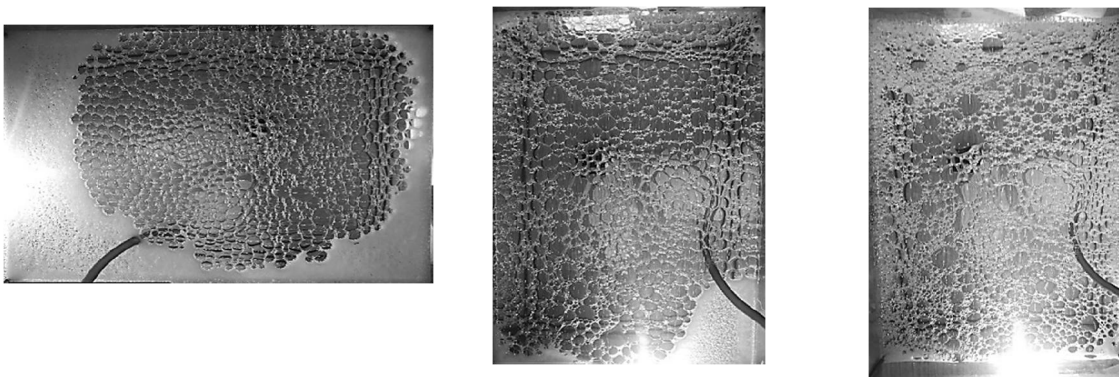


Figure 42 : foam at 10 [l/hr](left).50 [l/hr] (middle) and 150 [l/hr] (right)

size and median size of bubble, it was found that a low rate of 10 [l/hr] would create a good bubble size distribution in the middle of the liquid surface yet as the bubble goes away from the surface it was noticed that the bubble size drastically decrease, such surface foam would be hard to use in an industrial application, next in line was the median flow rate 50 [l/h] as it was noted that the foam median bubble size was better distributed around the liquid surface, lastly a high flow rate of 100 [l/hr] was used, and in such case there was a good distribution of bubble size on the surface on the fluid, yet too much of the bubbles merged due to the high velocity of the bubbles. The median flow was considered the best for the next step of Digital image processing.

4.3.3 Digital Image processing

By digital image processing it's possible to identify a lot of differences hidden from the human eye, usually due to subtle details that needs to be measured, or

the high quantity of data that needs to be extracted, one of the applications of Fourier transform is using it to extract edges of an image, such method usually used for periodic signals, to simplify it into more simple harmonic equations.

Wet foams are a good point for study because it is considered an intermediate point for the forming of metal foam, wet foam studies have been used extensively in predicting the behavior of macro porous ceramics, and used to

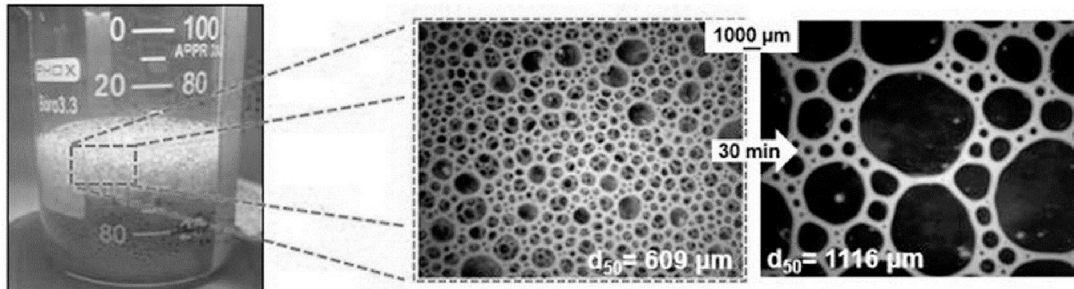


Figure 43 digital image analysis of generated foam [6]

control the porosity of the end product, the idea behind macro porous ceramics is similar to the idea of metal foam, in which a surfactant is used to improve the stability of wet foams [66], surfactants are frequently used to decrease the surface tension by adsorption at the air-liquid interface, modifying the viscoelasticity of the interfaces and inducing repulsive forces between bubbles, and thus increase the lifetime of air bubbles, due to the huge number of bubbles to be analyzed means of digital image processing is used, in one study the effect of the average bubble diameter due to agitating stirring was demonstrated by digital image software ImageJ, result of image analysis is shown in where average foam diameter change from 609 μm to 1116 μm after 30 mins of stirring [67]

Using digital Image processing software it was possible to extract contours of the bubble shapes and by means of calibration of the camera, it was possible to calculate the frequency of occurrence of certain bubble diameter sizes, this was laid out in the Histogram above, the image processing software is capable of turning the image to a binary one, then using tools for decreasing noise, and measuring the circularity it was possible to measure the bubble diameter, Fig shows the outlines of the bubbles, highlighted in black. This histogram would

be of aid in determining the average cell size in the manufacturing of metal foam,

4.3.3.1 Stages of extracting data from an image

4.3.3.1.1 An Image histogram:

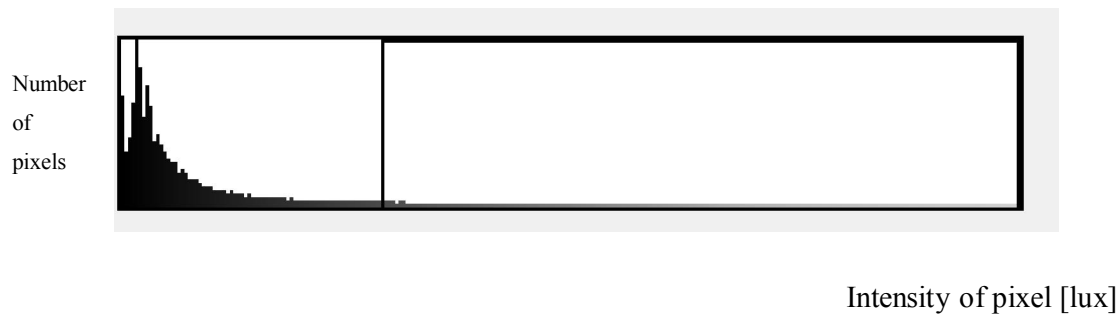


Figure 44 Histogram of a photo

For a greyscale image, it's composed of pixels depending on the resolution, an 5184 3436 rows, 8 million pixel, each pixel will have an intensity somewhere between 0 and 255, if we count the number of pixels of every intensity, then we can create a plot with a vertical bar of number of pixels and a horizontal scale of the intensity value ranging in between 0 and 255, by a histogram we can determine the number of pixels with the corresponding intensity, it could be helpful to check the an cumulative insensity graph to determine where most of the pixels lie, a brighter picture will have more pixels with higher value of intensity (closer to right, the value of 255)

From the histogram it is possible to determine if an image has a high contrast where the values (number of pixels) on the histogram will be divided equally on the left and the right of the histogram, while a low contrast image will have most of the values of the intensity of the histogram will be in the middle

4.3.3.1.2 Low pass filter for edge detection:

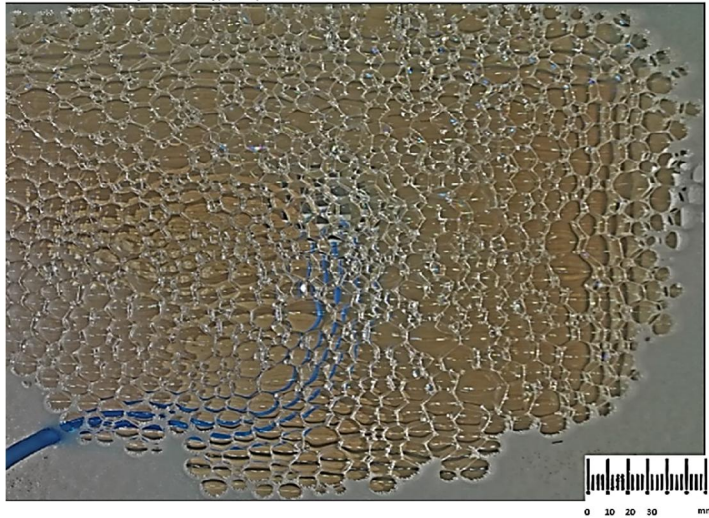


Figure 45 image after low pass filter

What Fourier transform does is that it transform a signal into an alternative representation of sine and cosine waves, by using a Fourier transform of the image as a mask, it is possible to highlight the edges of the picture, also known as a low pass filter

4.3.3.1.3 image thresholding

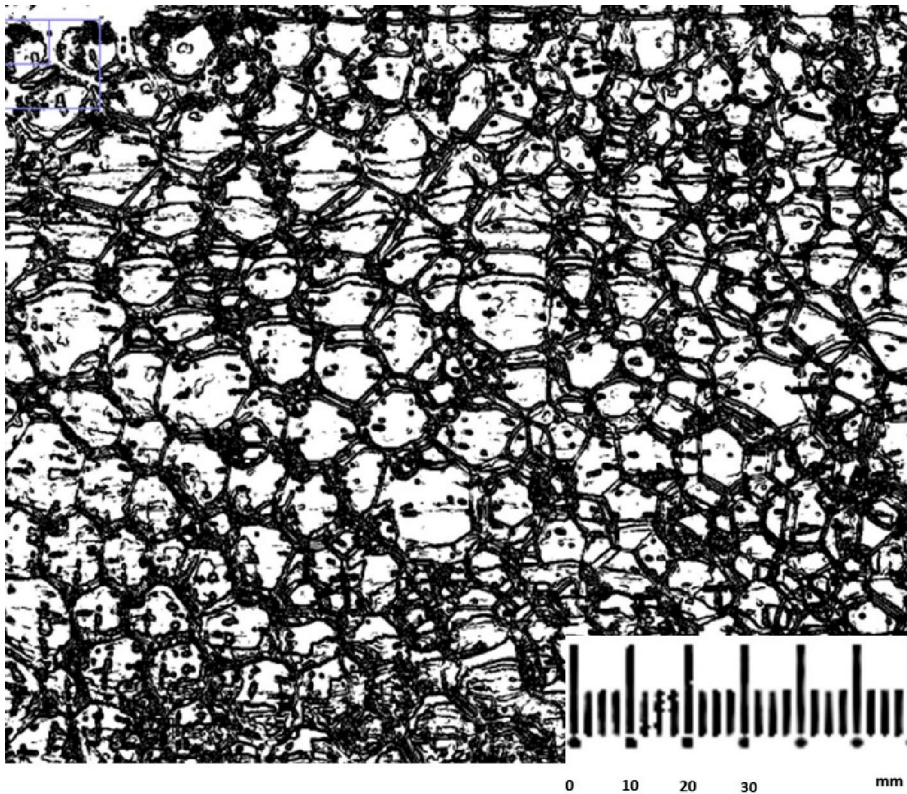


Figure 46 segmented image

image segmentation is when a photo is processed in order to show different parameters within an image, it's a way to understand what's going on in an image, image thresholding is a way to create a binary image of an image based on its histogram, what happens is by assigning a certain value in which the image on the histogram, in which all pixels having an intensity value before this number are turned off and the image is turned into a binary image with all values of all pixels in the image are either 0 or 1

4.3.4 Foam Analysis experiment

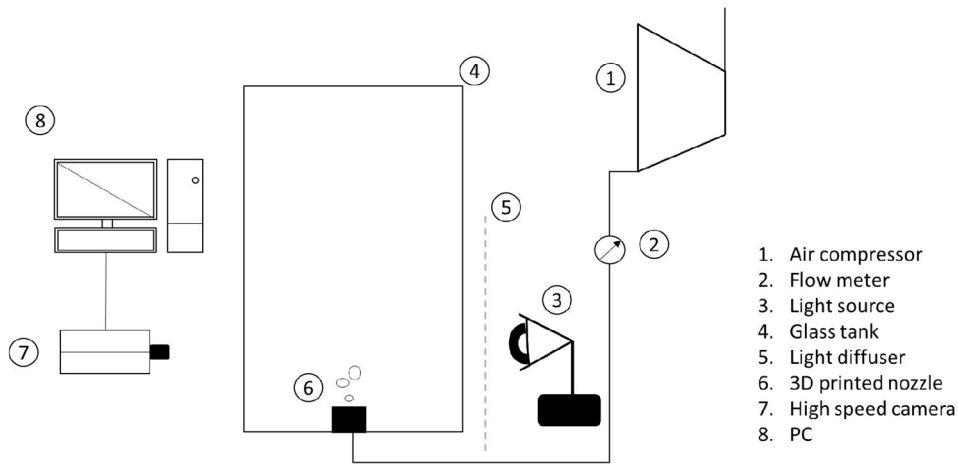


Figure 47 experiment setup for foam analysis

The experiment was done by injecting air into the water ethanol solution, for 60 seconds, after the end of the 60 seconds a picture was taken as parallel as possible and then this picture was processed through digital image processing software, then represented through various bins in which the diameter is represented under the bin that has the closest to the bin.

Solution properties:

Table 10 solution properties

| | |
|------------------------|----------|
| Surface Tension (mN/m) | 31 |
| Morton's Number | 5.60E-09 |
| Kinematic Viscosity | 2.14E-06 |

4.3.4.1 Foam bubble analysis: 10 l/ hr

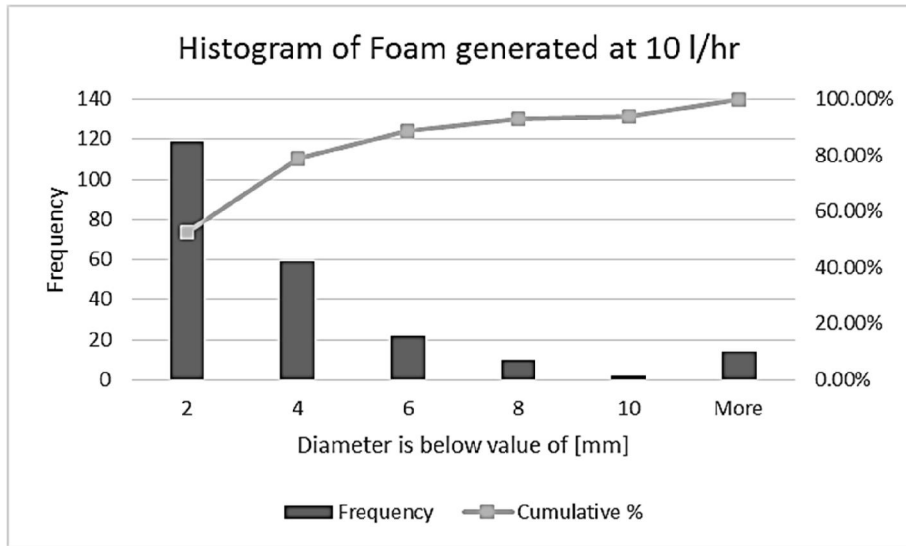


Figure 48 Bubble diameter distribution for 10 l/hr

For air injected into the mixture with flow rate of 10 l/hr most of the bubbles had an average diameter below 2 mm, with few bubbles exceeding 6 mm

4.3.4.2 Foam bubble analysis: 50 l/ hr

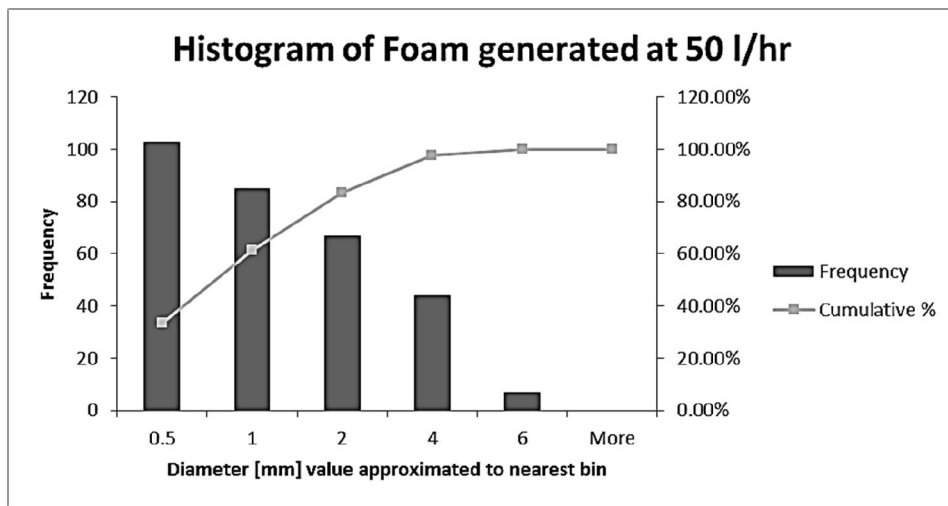


Figure 49 Bubble diameter distribution for 50 l/hr

For the flow rate of 50 l/hr, smaller bubble size was the dominant, with the highest frequency observed at 0.5 mm diameter,

4.3.4.3 Foam bubble analysis: 100 l/hr

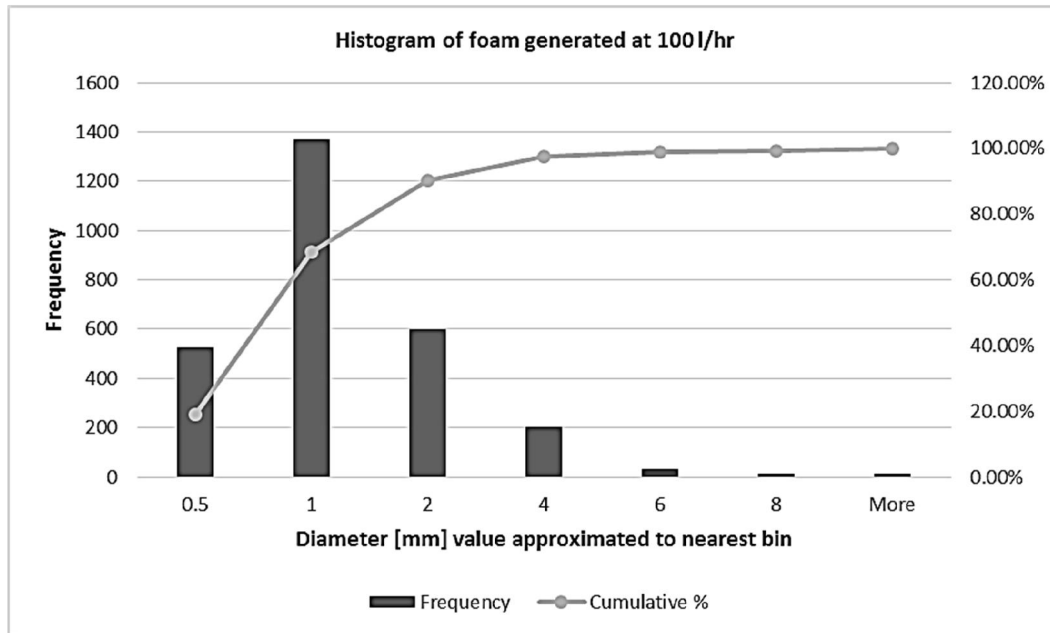


Figure 50 Bubble diameter distribution for 100 l/hr

For the highest flow rate it was observed once more that bubbles of the foam seem to stabilize around the same value if 1 mm in diameter

4.3.5 Analysis uncertainties:

With every method comes its own benefits and uncertainties and margins of error, and that's why it is essential to perform some qualitative analysis of the performed results

The method of edge detection for digital image processing works by finding the different values of contrast, this causes the method to not perfectly detect the edge of the bubbles in case of light reflection or refraction, this was avoided by using "fill holes" command, in this command the digital image processing software find the edge with less intensity value in the histogram and eliminates it, the difference could be noticed in the attached Figure 51 the

bubble area in black and the bubble boundary is shown in white, the command aids in removing all the white noise due to light reflection and refraction through the bubble and decreases the error.

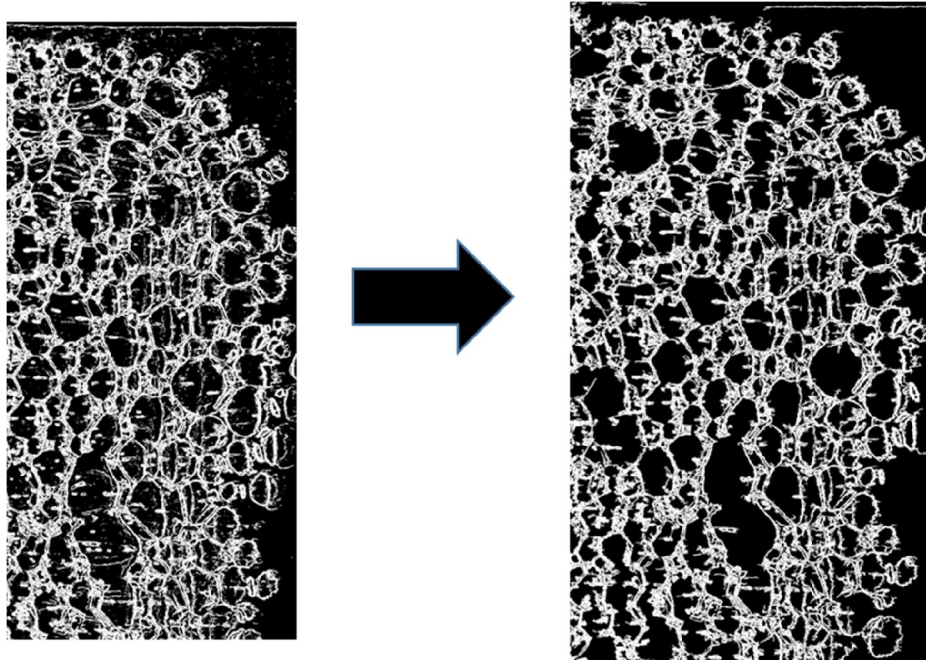


Figure 51 comparison for the same picture, before using fill holes command (left) and afterwards (right)

Another factor to consider for qualitative analysis is that bubble foam could be best described as a ellipsoid, as a 3D body with non-uniform diameter, in this method the geometry was approximated to a 2D circle with a uniform diameter, several studies recommended overcoming this error by using 2 camera and calibrating them to have an accurate 3D profile of the generated bubble, whether under the liquid surface or at surface of the liquid.

4.4 CFD Study for bubble under the surface

In means to aid the prediction of behaviour of bubble for the generation of metal foam, computational fluid dynamics were used in means of aiding such prediction, CFD is mainly used in simulation hard to reproduce scenarios from a simple stress abuse set-up to even more complex simulations for example fusion reactions in the sun, after studying a relation between the shape of

bubble under the surface of liquid, and the patterns made by the surface foam, it was an important step to start simulating the shape of the foam generated by an aluminium melt. No open publications were found studying the flow variable effects on the produced foam cell size and cell wall size. There is difficulties studying such parameters in a laboratory environment due to high temperature, oxidation and lack of transparency of the metallic melt. Computational fluid dynamics has become a very important and powerful tool for investigating and understanding flow phenomena.

Metal foam produced by gas injection has been simulated limitedly by other researchers, like Three-dimensional CFD simulation of bubble-melt two-phase flow with air injecting and melt stirring by [68]. in which a CFD simulation of a gas bubble metallic melt was simulated as a turbulent flow due to the effect of stirring by an impeller, a typical Metal foam production process, later on the through Multiple Reference Frames method, average bubble size is predicted, coalescence of bubble is taken into account using a transport equation. The study used a polyvinyl alcohol solution model to predict behaviour of AL melt, study concluded that an increase in the impeller speed increased the gas volume fraction, yet decreased the bubble average size.

The two-phase flow problem emerges in many technical applications starting from production processes up to the energetics. The objective of this two-phase flow examination was motivated by the effort to understand and further control the bubble formation in the metal foaming processes. There are generally many technological production methods to obtain the cellular type structures e.g. the continuous gas injection in the melted materials containing mostly other stabilization components. Details about aspects of the cellular material production can be found e.g. in [69]. This research is concerned with the study of rising gas bubble in stagnant liquid in pursue of creating metal foam, where common parameters such as gas bubble diameters, velocity and dimensionless parameters and Morton number were examined. Other non-dimensional relevant parameters used in the problem of the bubble dynamics investigation can be found in [70]. To validate the numerical results, two

different experimental examination patterns defined by the Morton numbers 1.6×10^{-11} and 5.7×10^{-9} were tested. It was found experimentally, that for the higher Morton number it was possible to trap the gas bubbles under the surface of the liquid, while for the latter it was not possible to trap any gas bubbles under the surface of the liquid fluid. The numerical approach based on the a multi-phase flow model which was built on the conservation laws of mass, momentum and energy as well as the gas-phase volume fraction advection equation was successfully adopted for the bubble formation problems [71] In the study of bubbles in [72] involving the dynamics of a bubble, it was found that the deformation predicted using the numerical calculation was a good fit for the experimental results. It also confirmed the dependence of the bubble aspect ratio on Weber and Morton numbers for the cases of spherical and ellipse bubbles. CFD approach was successfully used for prediction of the bubble formation in the bubbly liquid metal flows. The chosen numerical method is an immersed boundary method extended to deformable bubbles. Experimental and numerical results were found to be in very good agreement both for the disperse gas phase and for the continuous liquid metal phase [73]. Other techniques used for the multicomponent two-phase fluid mixtures in a closed system at constant temperature can be found in [74]

4.4.1 Boundary conditions

Fluid Surface tension: 72 mN/m

/flow rate: 130 l/h

The geometry was modeled as a slice of the tank used for the experiment, a 2D surface was created with 200 mm x 300 mm with a nozzle in the center with the diameter of 3 mm.

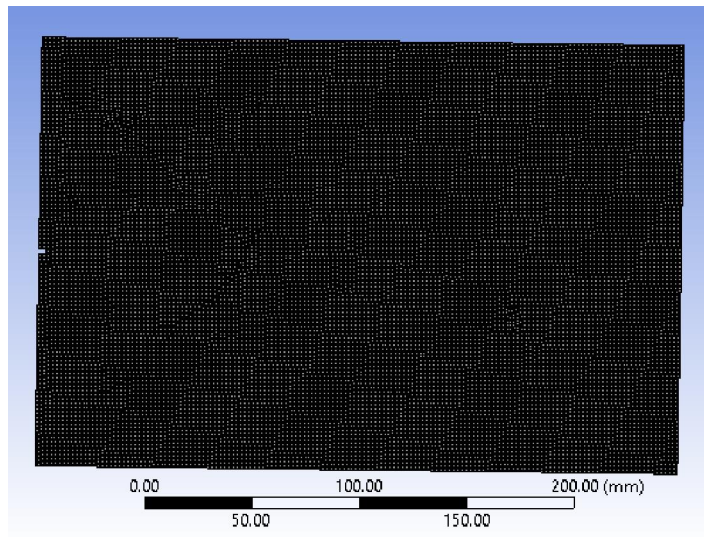


Figure 52 Mesh created

For meshing it was expected to have smaller element size closer to the nozzle inlet, which was added to the mesh with a custom mesh sizing command

4.4.1.1.1 Mesh statistics:

Elements: 60036

Average aspect ratio of elements is 1.006

Average Skewness 6.9E-003

4.4.1.2 Solver

ANSYS offers 2 different types of solvers Density based and Pressure based, and while as the software is getting more advanced they are trying minimize the gap between the two solvers, yet the two solvers operate with an intrinsically different nature, the density based solver couples equations of Energy, momentum and continuity together and solves them simultaneously [75] which requires more time and memory, yet could provide more accurate results for simulations with supersonic velocities and highly varying density. For our simulation here we assumed the pressure increase at inlet is of linear function increase, so the difference between pressure at inlet and pressure

inside the bottle is low enough for us to use the pressure-solver, which should need less time for the calculation to be finished; A variant of the pressure solver shall be used, by the name of The Pressure-Based Coupled Algorithm, this solver couples the momentum and continuity equations, then solves the rest of the governing equations sequentially in a segregated method that means it doesn't require as much memory as the density based solver

4.4.1.3 Turbulence Model

Viscous K omega turbulent model

The SST $k-\omega$ turbulence model is a two-equation eddy-viscosity model which has become popular in CFD [76]. The shear stress transport (SST) formulation combines the use of a $k-\omega$ formulation in the inner parts of the boundary layer makes the model directly usable all the way down to the wall through the viscous sub-layer, hence the SST $k-\omega$ model can be used as a Low-Re turbulence model without any extra damping functions. The SST formulation also switches to a $k-\epsilon$ behaviour in the free-stream and thereby avoids the common $k-\omega$ problem that the model is too sensitive to the inlet free-stream turbulence properties. Authors who use the SST $k-\omega$ model often merit it for its good behaviour in adverse pressure gradients and separating flow. The SST $k-\omega$ model does produce a bit too large turbulence levels in regions with large normal strain, like stagnation regions and regions with strong acceleration. This tendency is much less pronounced than with a normal $k-\epsilon$ model though

4.4.1.4 Volume of fluid Model

Volume of fluid is used to model 2 or more fluids by solving their momentum equation, while recording the changes to the volume fraction of the mesh domain, it is used for predicting the movement of an air bubble in liquid, in the current simulation the primary phase was defined as water, while the secondary phase was defined as air. It is recommended to use double precision when calculating multiphase flows, given that the surface tension is essential

for determining the shape of the bubble, it was taken into consideration with a given value of 72 mN/m.

VOF Model is used for solving inhomogeneous multi-fluids, in which momentum, energy and turbulence equations are calculated for each phase separately'

4.4.2 Results (volume fraction contours):

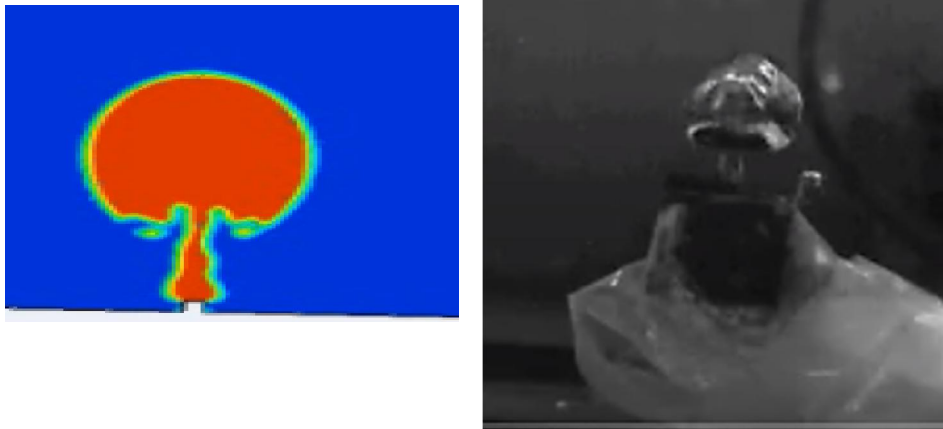


Figure 53 simulation vs speed camera shape bubble, nozzle exit

Figure 53 shape acquired through CFD simulation is a visual match, with the actual shape acquired by the speed camera, this is the first stage of bubble formation, air is injected into the main bubble with no to low resistance, also the bubble hasn't reach the critical volume in which buoyancy forces would cause the rapid increase in the velocity the diameter ratio $\left(\frac{D_{sim}}{D_{exp}}\right) = 1.4$

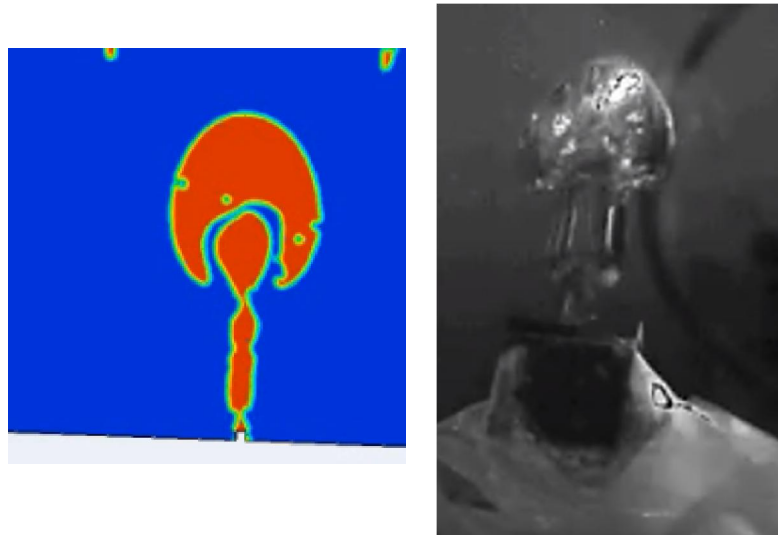


Figure 54 econd stage of bubble leaving nozzle area

At this phase the bubble has reach a critical volume value, and it starts to ascend with a higher velocity to the surface of the liquid, at this stage buoyancy forces are highly influencial here,

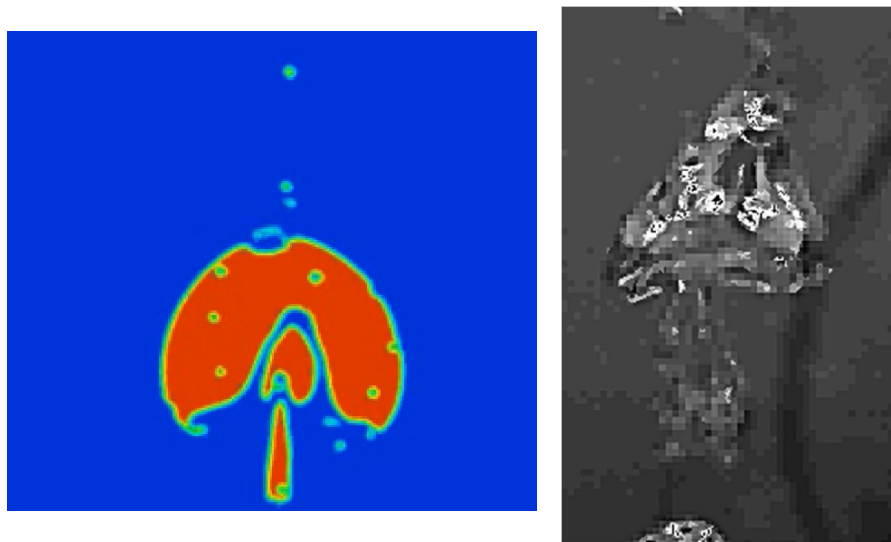


Figure 55 simulation vs experiment for bubble merging

It was noticed in both simulation and experiment that the bubble after separation from the nozzle decelerates somewhere in the middle of the tank,

and merge with other smaller bubbles, the phenomenon of bubble merging could be reduced by adding a surfactant [33]

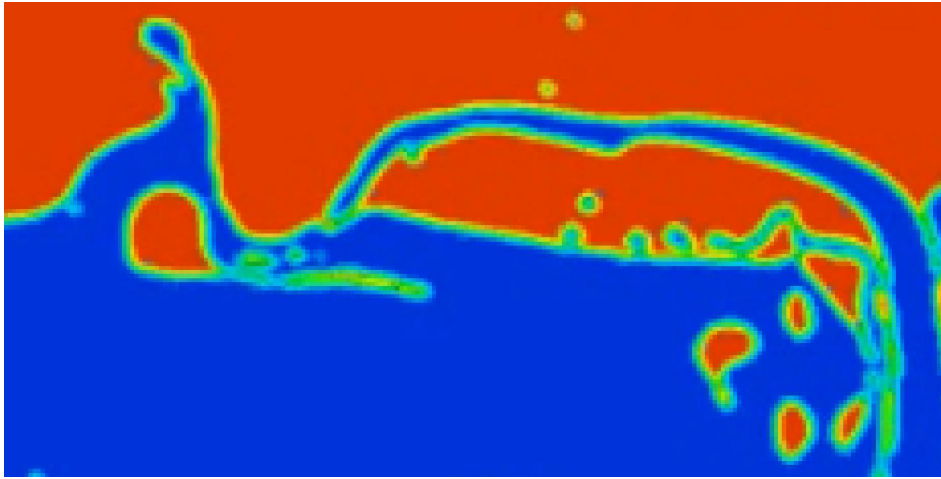


Figure 56 Liquid surface disturbance CFD vs Experiment bubble surface breakage

As the bubble approaches the surface at this flow rate at tested flow rate (130 l/hr) it usually causes a high turbulence in the fluid, this disturbance could be noticed in both experiment and simulated results.

4.4.3 Simulation Model validation (Bubble diameter):

3 different simulations were made with same boundary conditions, same geometry dimensions the only difference was the mesh, to notice the effect of grid size as well as having a 3D mesh instead of a 2D one, a comparison of the simulation parameters could be found in the below Table 11 simulation criteria

Table 11 simulation criteria

| | 2D | fine | 2D | Coarse | 3D |
|-----------------------------------|-----------------------------|------|-------|--------|--------|
| Mesh Elements # | 58417 | | 26301 | | 372891 |
| Solver | Pressure based | | | | |
| time | Transient | | | | |
| gravity [m/s ²] | 9.81 | | | | |
| Multiphase model | VOF (2 Eulerian phases) | | | | |
| Courant number | 0.25 | | | | |
| Phase interaction model | Surface Tension Force Model | | | | |
| Surface tension coefficient [N/m] | 0.072 | | | | |
| Boundary conditions: | | | | | |
| inlet velocity [m/s] | 0.15 | | | | |
| inlet diameter [mm] | 3 | | | | |
| Solution methods: | | | | | |
| Pressure-velocity coupling | SIMPLE | | | | |
| Pressure Discretization | PRESTO! | | | | |
| Momentum Discretization | Second Order Upwind | | | | |
| Volume Fraction Discretization | Geo-construct | | | | |
| Turbulent kinetic energy | Second Order Upwind | | | | |

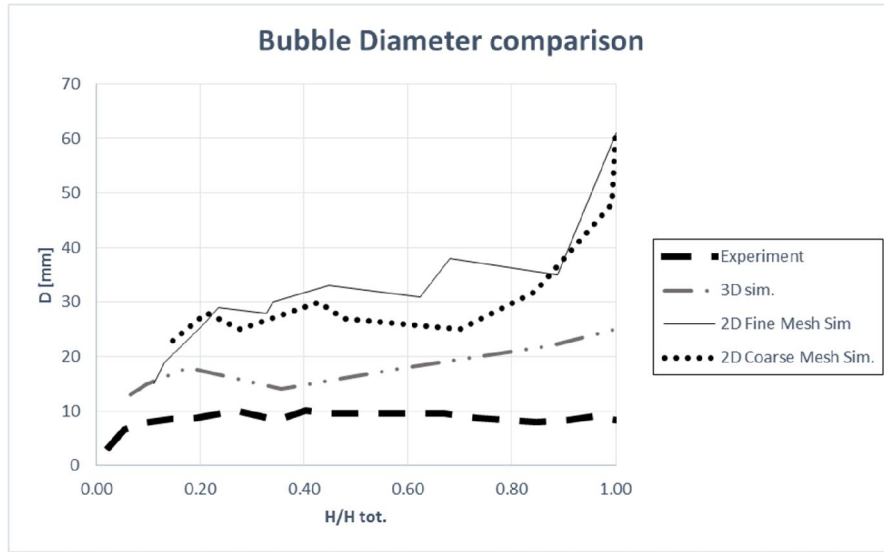


Figure 57 bubble size comparison

Figure 57 shows the results from the rising bubble in stagnant flow, from experimental observation the bubble has almost little to none increase in the bubble diameter once crossed half the total height (H_0), while in all simulations it was expected to increase drastically in size, when comparing the mesh element size, it is noticed that having a 3D mesh has the most substantial effect on the correct prediction of the bubble diameter.

4.4.4 Effect of flow rate on foam pore size

The study of rising bubble in liquid has been proved to influence the pore size in the metal foaming process, it was noticed that as the bubble rise it expands due to the decrease of acting pressure on the bubble, the bubble could stop the ascend in the liquid of molten metal when equilibrium has been reached, or alternatively when the metal has fully solidified a slice of the foam solid represents an instant of the bubble where it is stuck.

Through the study of change in the bubble size as well as other parameters, it is possible to predict the size of the pore as it is correlated to the size of the rising bubble in the liquid, it was also noticed that by using a lower flow rate a

smaller gas bubble is usually conceived in the liquid medium, resulting in a smaller pore size.

5 Equipment Design Concept for Metal foam Production

Based on the values obtained through lab experiments, a design concept was created to produce metal foam, the concept takes the best values of viscosity, flow rate and bubble distribution obtained by digital image analysis. Concept is to have molten aluminum in a tank, while compressed air is pushed inside the molten liquid as the metal solidifies the air bubbles would be stuck inside the mixture; simultaneously additives are added and mixed by using the impeller.

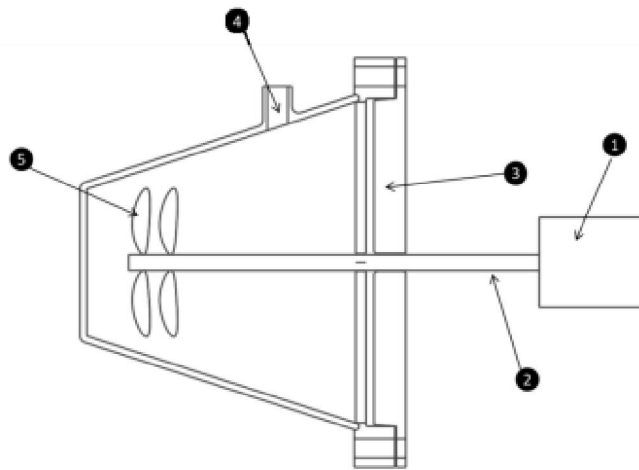


Figure 58 sketch of design concept

1. Motor for gas propeller
2. Shaft connecting rotor with propeller, with an inner tube for pressurized inert gas
3. Pressure tight cover
4. Vent for equalizing pressure
5. Propeller for propagation of gas bubbles

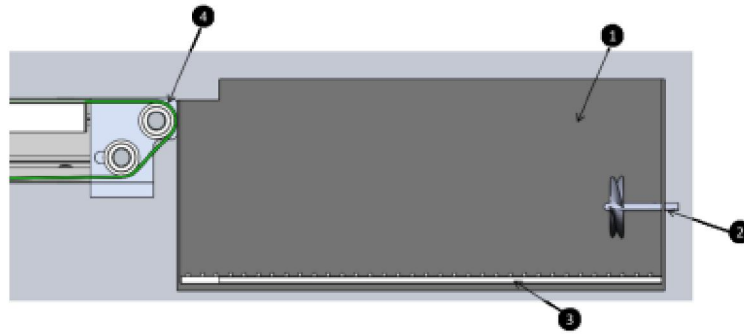


Figure 59: 3D CAD Model of Equipment's concept

1. Tank for molten metal
2. Propeller / impeller
3. Nozzle mesh plate
4. Conveyor belt (available solution)

5.1 Operation conditions:

Based on market available solutions, and study made in this research metal foam conditions are proposed: a mixture of 6061 Al-alloy and SiC is melted at 680 °C, the SiC particle size should be around 5 μm for easy mixing, with volume fraction of 5 to 7 %, once the mixture reaches the required temperature, the impeller is required to rotate from 600 to 700 rpm with an air flow rate of 8 to 10 l/min per one nozzle, then heating should only be continued at the bottom of the foaming tank the top layer of the tank will solidify and using external force could be moved onto a heat resistance conveyor belt, this technique is expected to produce Aluminium foam with porosity 75 to 95%, a non uniform cell size.

Through the carried out experiment in Page 32 it was concluded that without the usage of a surfactant to modify the properties of the liquid an excess of bubble merging occurs, a surfactant depending on the type of metal is essential to maintain the generated bubbles at the same size, otherwise coalescence happens and metal foam ends up with a bigger cell size than requested.

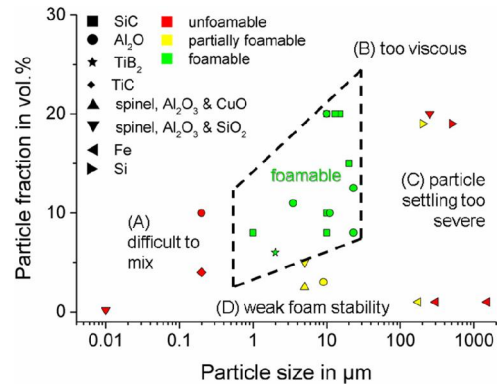


Figure 60 usage of surfactants for foaming different metals [92]

While through digital foam analysis on page 65 it was concluded that a lower flow rate would generate a more uniform surface foam on the surface, with a lower cell size due to the smaller size bubbles generated.

Finally though the CFD simulation on page 68 it was concluded that merging would occur in bubbles if no surfactant was added to the molten liquid, and a lower flow rate would decrease of the velocity of the bubbles aiding in the stabilization of the bubble in the liquid.

5.2 Components Created:

5.2.1 Molten Metal tank:

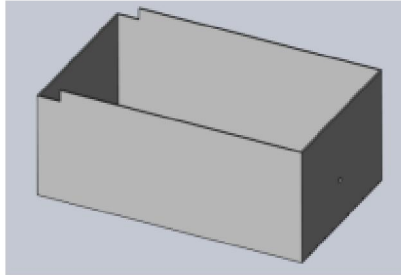


Figure 61 Molten metal designed tank

The tank where molten aluminum would be poured, the tank was designed to be connected to a conveyor belt, to transport solidified bubble filled metal, on the other side the tank has one hole for impeller to be fit with bearings as well as 10 holes for connection of gas tubes, the height (dimension in direction of gravity) is minimized to keep the injected bubble at smallest size before reaching the solidification phase.

5.2.2 Propeller

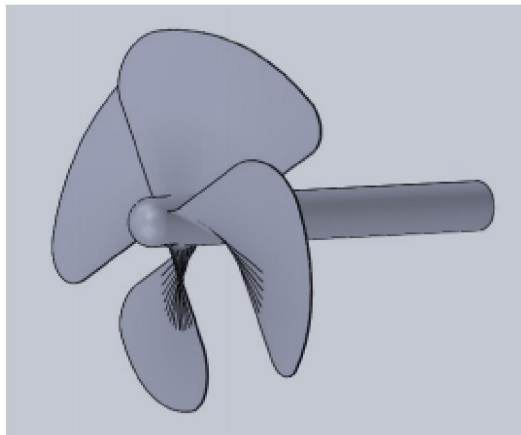


Figure 62 Propeller geometry

Propeller is used to make sure bubble propagation is homogenous, shown propeller is a market already available solution, one chosen had a diameter of 30 mm. the impeller is expected to rotate at 600 to 700 rpm. It was shown that maintaining lower flow rates, as much as adding a surfactant would help in good propagation of the bubbles in the melt.

5.2.3 Nozzle mesh plate

It's a hollow plate fit with 640 x 1.5 mm Diameter nozzles, to uniformly cover the whole bottom of the metal container, plate has slot from one side as inlet of inert gas.

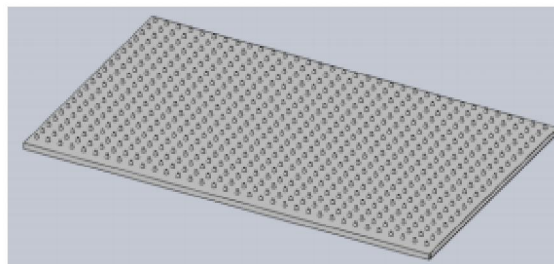


Figure 63 Nozzle mesh plate

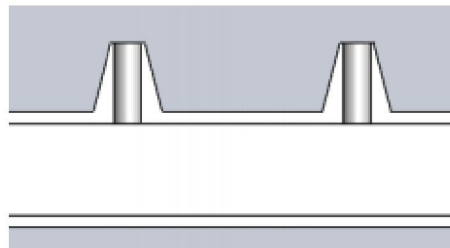


Figure 64 nozzle design close up

The concept of having several nozzles was proposed after the analysis of experimental results and noticing that passing a high flow rate through one nozzle ended with having a bad propagation of bubbles, as well as an increase in bubble coalescence, hence the design of multi nozzle was introduced in aim

to have a low flow rate (around 10 [l/hr]) per nozzle, to have bubbles with lower speed and more easier to stabilize in the melt.

5.2.4 Conveyor belt

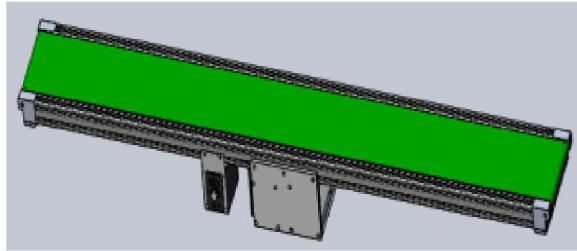


Figure 65 Conveyor belt

Conveyor belt is available as ready-made solution; preferably the belt would be made of stainless steel chains to be able to handle the temperature of the recently solidified aluminum

6 Metal Foam prepared at TUL



Figure 66 foam prepared at TUL

As part of the hybrid materials for hierarchical structures project it was possible to product Al foam in the university lab

The foam was prepared by gas injection into the aluminum melt, an aluminum magnesium alloy was used for the metal, later one a surfactant was chosen with volume percentage of 10 to 20 volume per cent of SiC or Al₂O₃ particles (particle size 5 to 20 micrometers) are used.

Prior to the foaming process by gas injection the particles were evenly distributed in the melt by mixing the melt by some impeller (1000 rpm for 10 to 15 minutes), while gas bubbles were fed into the melt from the bottom of



Figure 68 Al melt oven



Figure 68 mixing shaft and impeller

the container.

In another experiment [77], another way was presented to manufacture porous metal foam, the mixture of heat and pressure was used to melt aluminum alloy with NaCl as a space holder, and while there were other studies that relied only on compression to create the foam, this experiment should lead to a more homogenous mixture since the aluminum is melted under pressure, the experiment used Al alloy EN AC-44300 AlSi 12 (melting point approx. 577 °C), The chemical composition of used aluminum alloy AlSi12 was identified by a Bruker Q4 Tasman optical emission spectrometer, composition could be seen in Table 12

Table 12 chemical composition of used alloy [77]

composition of EN AC 44300 alloy wt %

| Si | Fe | Mn | Cu | Zn | Ti | V | Mg | Na | Pb | Al |
|------|------|------|------|------|-----|-------|-------|-------|-------|-------|
| 12.1 | 0.43 | 0.46 | 0.04 | 0.12 | 0.1 | 0.007 | 0.001 | 0.005 | 0.004 | 86.96 |

The Alloy was melted in a crucible in a furnace of a varying temperature between 720 and 750 ° C , then the molten metal was poured in a preheated mold, finally a measured amount of Sodium chloride was added and the mold was inserted under a hydraulic press, the pressure was around 80MPa.



Figure 70 different particle size used for NaCl place holders for the metal foam, 9 mm left, 6 mm middle and 4 mm right [77]

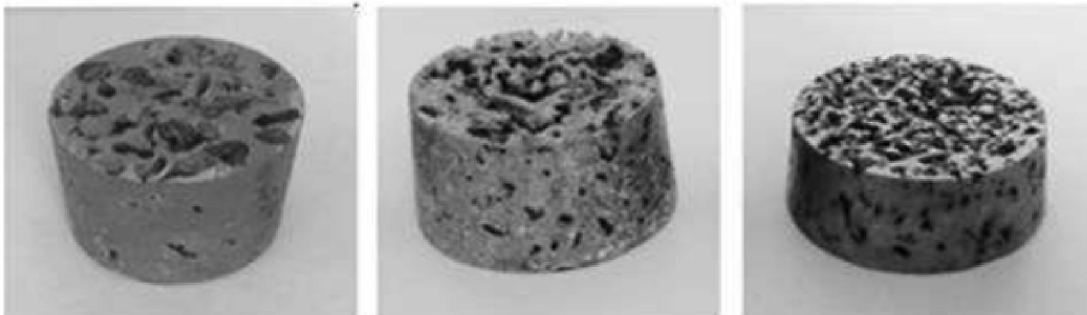


Figure 69 samples produced from the procedure: 9 mm place holder particle size on the left, 6 mm in the middle and 4 mm on the right [77]

Different average size for space holder particles were used: 9 mm, 6 mm and 4 mm Figure 70, that affected the produced metal foam with varying pore size, in Figure 69

The study later proposed stress strain testing curves of the created specimen and suggested for the production reasons a 50% Sodium chloride to 50% Al alloy on volume basis to be used for production purposes, the porosity of the samples or produce could be controlled between values of 59 to 64% and the

density could be varied between 950 to 1085 Kg/m³ . this study could be compared as well to another study published in Athens Journal of Technology and Engineering [50] in which used scrap Aluminum Alloy EN AW 2011 waste chips was mixed with different placeholders, like Himalayan salt, urea and table salt with average particle size of: 5.2, 1.48 and 4,7 mm respectively, in this experiment a vibrating mechanism was used to help make the samples homogenous with the place holders, and since only scrap was used it was only needed to compress the material instead of melting. A slightly different alloy was used with composition in that study the alloy has more copper which could be the reason the scrap is more ductile and could be compressed easily instead of melted.

Table 13 chemical composition of used alloy in Study [50]

composition of EN AW 2011 alloy wt %

| Si | Fe | Mn | Cu | Zn | Ti | V | Mg | N a | Pb | Al |
|------|-----|--------|------|-------|--------|---|-------|--------|-------|---------|
| 0.14 | 0.5 | 0.0225 | 5.66 | 0.012 | 0.0059 | 0 | 0.015 | 0 | 0.586 | 93.0586 |

While in the first study the place holder particle were measures to take 50% of the volume, in that study it was decided to have 60% on mass bases of the space holder, another point of different the study made in Liberec highlighted that the pressure should be around 80MPa, the latter study highlights that a 500 kN force was exerted on a sample of diameter 40.2 mm, making the pressure 393 MPa, also the specimen was left in boiling water for half an hour to remove the space holder salt, this enabled the created foam to have density ranging from 1086 to 1259 Kg/m³ . When one feature of the cold pressing technique is that plastic deformation occurs and that leads to an increase in the hardness of the final sample, also the compression strength was measured in both studies, the latter having the highest compressive strength at 30.8 MPa for the sample prepared with urea space holder particles, while for the samples prepared by melting the value was much higher.

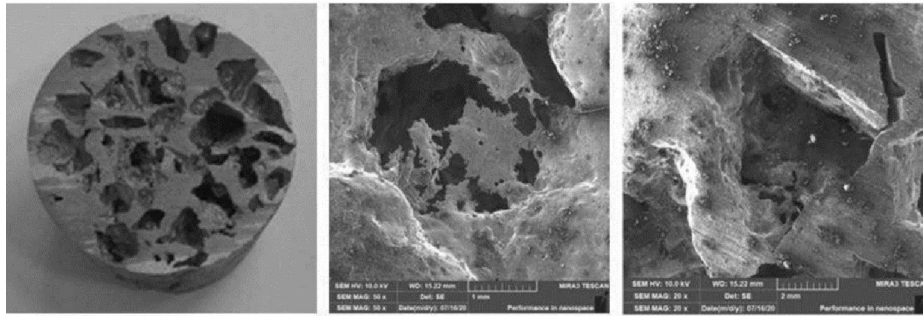


Figure 71 photos from microscope for investigating Al sample with 9 mm sodium chloride [77]

In the Liberec study the samples were investigated using an electron scanning microscope Figure 71

to investigate the effect of the inner structure on the compressive strength of the affected porous metal samples, the study concluded that the larger sodium chloride particles created larger pores in the material, and that affected the compression strength value negatively

7 Conclusion

The process of metal foaming by direct gas injection has some similarity with the used experiment test rig, as both use some sort of a nozzle to directly inject a gas in a liquid, yet it could be noticed that there are several differences that would make correlating the behaviour of a gas bubble in the molten metal hard, both liquids would have different values of viscosity, surface tension and density, yet by means of monitoring those factors in water ethanol mixture, it is possible to find how such factors are interdependent and thus influencing the process of metal foam.

An experiment was carried out by the usage of a speed camera and image processing software to monitor the different shapes of a gas bubble rising in stagnant liquid, where properties like aspect Ratio, diameter of the gas bubble, velocity could be evaluated in relation to changing the viscosity, density and surface tension of the stagnant liquid and described through the postulation of dimensionless parameters like Reynolds, Morton and Eötvös. Water was used as one of the stagnant liquids, while the other liquid used was water-ethanol mixture to influence the viscosity and surface tension, through this experiment several conclusions could be observed.

Eötvös number increases as the rate of flow rate increases, as there was a significant increase in the values of Eötvös number (10 to 55) when the flow rate was 130 l/h, while when the rest of the results were acquired at an air volume flow rate about 15 l/h Eötvös were around 1, a much higher values than one could indicate that the dominant factor influencing the shape of the gas bubble is gravitational force, which could also be linked that at a higher flow rate the size and also the mass of air bubbles is higher.

It is also noticed that the effect of bubble merging depends on both the flow rate and the fluid properties, as for the first acquisition at 130 l/h, bubble merging was prevalent that is seems that isolating a single bubble for analysis was hard, and at the 15 l/h it was easier to analyse a single bubble, yet there

was dependency on viscosity and surface tension since when ethanol was added to the water, even at a low flow rate of 15 l/h merging between the air bubbles occurred

When comparing from the perspective of Morton's number, it could be said that for a Morton's number of 1.595×10^{-11}

It was possible to trap air bubbles under the surface of the liquid, no interference occurred between the air bubbles, but at same nozzle diameter (3 mm), flow rate 15 l/h, but changing viscosity, surface tension and density making a Morton's number of 5.658×10^{-9} bubbles were not trapped under the liquid surface, while interference still happened between the bubbles.

It is noted that adding ethanol into water increases the chance of having foam.

Measuring the effect of ethanol on the water could also be noticed in how the surface tension and viscosity change, as in figure the viscosity increases till a molar fraction of 0.21 is reached and then it decreases again.

As for surface tension it is noticed that after a molar fraction of 0.13 a drastic decrease of surface tension is observed.

By means of Digital image processing it was possible to analyse and measure thousands of gas bubbles on the surface of the liquid, and in a molten metal environment, this liquid surface would solidify leaving those bubbles as hollow spheres in the metal body, and properties such as viscosity and surface tension are essential to influence factors such as bubble size, and number of bubbles.

By the aid of digital image processing 3 different flowrates of foaming were analyzed for the flowrates 10, 50 and 100 l/hr, to obtain the average diameter of foam bubble formed, 10 l/hr had most bubble below 2 mm in diameter, 50 l/hr had a similar distribution which could mean the rate of flowrate isn't as

influential as much as the viscosity and the surfactant additive to create or maintain injected foam, lastly a flow rate of 100 l/hr was introduced which has a significant number of bubble below or equal to 1 mm which could be explain by the high turbulence that caused some of the bubble to disintegrate.

A CFD simulation was made to study the bubble shape under the liquid surface, it was described with volume fraction contours and the results were a good match with the high speed camera photos. With a diameters at of simulated bubble and experiment bubble had the same shape but with a 40% difference in diameter.

Finally, an experiment was made in the technical university of liberec to produce metal foam by direct gas injection in a heated aluminium pool, with Al₂O₃ alloy and Silicon carbide as a surfactant, the experiment yielded Aluminium foam, yet, and later on concept for equipment design was presented for foam production, the concept had 4 main components: tank, impeller, nozzle plate and a conveyor belt and this design be used

Through study of the behaviour of the bubble under the surface of the water, and foam formed on the surface of the liquid, it was possible to provide ways to analyse and inspect foam formation, and propose operating condition for the production of Aluminium metal foam.

8 List of Figures

| | |
|--|----|
| Figure 1 increase of radii due to interferential expansion between 2 fluids..... | 11 |
| Figure 2 the structural hierarchy of ligament and tendon [85]. | 14 |
| Figure 3 illustration of different types of Hierarchical Materials | 14 |
| Figure 4 comparison between different metal foams [3] | 15 |
| Figure 5 definition of foam..... | 16 |
| Figure 6 Variation of total time required for complete melting of PCM. | 20 |
| Figure 7 Aluminum honeycomb (left) vs Nomex (Right) [29] | 21 |
| Figure 8 Melt gas injection method [91] | 23 |
| Figure 9 Metal Foam by direct injection..... | 24 |
| Figure 10 Particle volume fraction, Size for foaming [36] | 25 |
| Figure 11 foam by gas agents | 27 |
| Figure 12 Metal foam by casting [46]..... | 28 |
| Figure 13 hydrogen solubility based on temperature [47] | 28 |
| Figure 14 foam production equipment..... | 29 |
| Figure 15 Experiment setup..... | 32 |
| Figure 16 photo from lab..... | 33 |
| Figure 17 Equipment used..... | 34 |
| Figure 18 Viscosity measuring equipment..... | 36 |
| Figure 19 Viscosity measuring equipment at TUL..... | 37 |

| | |
|--|----|
| Figure 20 lab measured viscosity (left), journal validated results [57] (right) | 37 |
| Figure 21 measuring Surface tension | 38 |
| Figure 22 Lab measured results (Top) independent journal results,of 3 different experiments each indicated by its own symbol [55] (Bottom) | 39 |
| Figure 23 Image processing software | 41 |
| Figure 24 Flow meter (manufacturer Manual) | 42 |
| Figure 25 3D printed nozzle | 43 |
| Figure 26 - Bubble shape change w time | 46 |
| Figure 27- bubbles trapped under water surface | 47 |
| Figure 28 rising bubble sequence | 48 |
| Figure 29 aspect ratio vs time | 48 |
| Figure 30-Eotvos values change with time | 49 |
| Figure 31 Re vs time for rising bubble | 49 |
| Figure 32 - Reynold's number values of nozzle diameter 3 mm and flowrate 130 l/h compared to D3V15 | 51 |
| Figure 33 - Diameter values of nozzle diameter 3 mm and flowrate 130 l/h compared to D3V15 | 52 |
| Figure 34 The predicted bubble shapes as a function of Reynolds and Bond numbers [64] | 53 |
| Figure 35 aspect ration change for a bubble rising in stagnat fluid [65] | 54 |
| Figure 36 Bubble shapes | 55 |
| Figure 37: Velocity vs Distance from nozzle | 56 |

| | |
|---|----|
| Figure 38 Aspect Ratio vs time..... | 57 |
| Figure 39 Re vs time | 57 |
| Figure 40 Eötvös vs time..... | 58 |
| Figure 41: Viscosity vs Ethanol Molar Fraction (left) – Surface tension vs Ethanol Molar fraction (Right) | 59 |
| Figure 42 : foam at 10 [l/hr](left).50 [l/hr] (middle) and 150 [l/hr] (right)..... | 60 |
| Figure 43 digital image analysis of generated foam [6]..... | 61 |
| Figure 44 Histogram of a photo..... | 62 |
| Figure 45 image after low pass filter..... | 63 |
| Figure 46 segmented image | 64 |
| Figure 47 experiment setup for foam analysis..... | 65 |
| Figure 48 Bubble diameter distribution for 10 l/hr..... | 66 |
| Figure 49 Bubble diameter distribution for 50 l/hr..... | 66 |
| Figure 50 Bubble diameter distribution for 100 l/hr..... | 67 |
| Figure 51 comparison for the same picture, before using fill holes command (left) and afterwards (right) | 68 |
| Figure 52 Mesh created | 71 |
| Figure 53 simulation vs speed camera shape bubble, nozzle exit | 73 |
| Figure 54 econd stage of bubble leaving nozzle area | 74 |
| Figure 55 simulation vs experiment for bubble merging | 74 |
| Figure 56 Liquid surface disturbtion CFD vs Experiment bubble surface breakage..... | 75 |

| | |
|---|-----|
| Figure 57 bubble size comparison | 77 |
| Figure 58 sketch of design concept..... | 79 |
| Figure 59: 3D CAD Model of Equipment's concept..... | 80 |
| Figure 60 usage of surfactants for foaming different metals [92] | 81 |
| Figure 61 Molten metal designed tank..... | 82 |
| Figure 62 Propeller geometry..... | 82 |
| Figure 63 Nozzle mesh plate | 83 |
| Figure 64 nozzle design close up..... | 83 |
| Figure 65 Conveyor belt..... | 84 |
| Figure 66 foam prepared at TUL | 84 |
| Figure 68 mixing shaft and impeller | 85 |
| Figure 68 Al melt oven..... | 85 |
| Figure 69 samples produced from the procedure: 9 mm place holder particle size on the left, 6 mm in the middle and 4 mm on the right [77] | 86 |
| Figure 70 different particle size used for NaCl place holders for the metal foam, 9 mm left, 6 mm middle and 4 mm right [77] | 86 |
| Figure 71 photos from microscope for investigating Al sample with 9 mm sodium chloride [77]..... | 88 |
| Figure 72 First bubble leaving the nozzle | 106 |
| Figure 73 bubble coalescence..... | 107 |
| Figure 74 mid tank height area, bubble experience a slowdown in velocity . | 108 |
| Figure 75 breaking out of the surface | 108 |

Figure 76 turbulence created by breaking the surface already affects the
generating of new bubble109

Figure 77 due to high turbulence, second wave of bubbles have a different
pattern of coalescence111

9 Bibliography

1. Roché M., Li Z., Marangoni Flow of Soluble Amphiphiles.. 2014, Physical Review Letters.
2. Li J. Nanocrystal Assembly of Hierarchical Porous Architecture for Photocatalysis. 2013.
3. Leistein, T., Jung, A. & Diebels microsphere-based material model for open cell metal foams. B. 2020, Continuum Mech. Thermodyn, pp. 255–267.
4. Sahoo v. Metallic foams: current status and future prospects. Jan 2006.
5. Bhatnagar, n. A survey of fabrication and application of metallic foams (1925–2017). July 2017, j porous mater , , vol. 25, pp. 537–554.
6. Banhart j. Manufacture, characterization and application of cellular metals and metal foams. December 2001.
7. Seeliger, banhart j. Recent trends in aluminium foam sandwich technology.,. 2012, advanced engineering materials.
8. Arenas j. P. Recent trends in porous sound-absorbing materials. S.l. : university austral of chile, jul 2010.
9. Leitlmeier. Metal foams – manufacture and physics of foaming. Jan 2003.
10. Heuss R., Müller N., van Sintern W., Starke A., Tschiesner A. Advanced industries: lightweight, heavy impact. S.l. : mckinsey Co.
11. D. Bhaga. Bubbles in viscous liquids: shapes, wakes and velocities. 1981, j. Fluid mech.
12. Grace, j.r. shapes and velocities of single drops and bubbles moving freely through immiscible liquids. 1976, trans. Icheme, vol. 54.

13. Maldonado, m. An experimental study examining the relationship between bubble shape and rise velocity. 2013, chemical engineering science.
14. Liu h., zhao g., experimental studies on the shape and motion of air bubbles in viscous liquids. April 2015, experimental thermal and fluid science.
15. Maxworthy, t. Experiments on the rise of air bubbles in clean viscous liquids. 1996, fluid mech.
16. Bothe d., fleckenstein s., a volume-of-fluid-based method for mass transfer processes at fluid particles. September 2013, chemical engineering science.
17. Gumulya m., bubbles in viscous liquids: time dependent behaviour and wake characteristics.. February 2016, chemical engineering science.
18. Ren, b., jiang, y., li, c. A simple approach for bubble modelling from multiphase fluid. 2015, comp. Visual media.
19. Tomiyamaa a. Terminal velocity of single bubbles in surface tension force dominant regime. 2007, world academy of science, engineering and technology.
20. Rayleigh l., on the pressure developed in a liquid during the collapse of a spherical cavity. 1917, the london, edinburgh, and dublin philosophical magazine and journal of science.
21. Hager. History and significance of the morton number in hydraulic engineering. 2014, journal of hydraulic engineering.
22. Viana f., pardo r., yanez r., universal correlation for the rise velocity of long gas bubbles in round pipes.. 2003, j. Fluid mech.
23. Parveez B., Maleque M. A. Review on advances in porous Al composites and the possible way forward.,. s.l. : Journal of Materials Research and Technology , July 2021.

24. Bondareva N., Sheikholeslami M., Sheremet MA. Temperature and convective heat exchange with an environment on heat transfer inside phase change material embedded brick. 2021, Journal of Energy Storage .
25. Nobrega C., Kar I.,Fam L., Solidification around axial finned tube submersed in PCM: modeling and experiments.. 2020, Journal of Energy Storage.
26. M. Abuşka, S. Şevik and A. Kayapunar. Experimental analysis of solar air collector with PCM-honeycomb combination under the natural convection. 2019, Sol Energy Mater Sol Cell, Vol. 195, p. P. 299.
27. Honeycombpanels. [Online]
<https://www.honeycombpanels.eu/en/products/honeycomb/nomex-aeronautical-grade-en>.
28. Yahya M.A, Ruan D., Response of aluminium honeycomb sandwich panels subjected to foam projectile impact – An experimental study.. 2015, International Journal of Impact Engineering, pp. 100 - 109.
29. [Online] <https://www.plascore.com/honeycomb/honeycomb-cores/aramid-fiber/pn2-aramid-fiber-honeycomb/>.
30. [Online]
https://www.plascore.com/download/datasheets/honeycomb_data_sheets/PLA_PAMG-XR1-5052_4-6-2021.pdf.
31. W Ruch, B Kirkevag. PCT/NO90/00115
32. Thomas M., Kenny D., Sang H. Particle-stabilized metal foam and its production . US5622542A 1993.
33. Deqing, W., Effect of ceramic particles on cell size and wall thickness of aluminum foam. 2003, Materis Science and Engineering.

34. Leitlmeier, D. Development of a Foaming Process for Particulate Reinforced Aluminum Melts. 2002, *Advanced engineering materials*.
35. Heim K. Particle size and fraction required to stabilise aluminium alloy foams created by gas injection. 2018, *Scripta Materialia*.
36. SRIVASTAVA V. Processing, stabilization and applications of metallic foams. *Art of science*. 2007, *Materials Science-Poland*.
37. 46. J., Banhart. 2001, J., *Prog. Mater. Sci.*,
38. Banhart J. Light-metal foams - History of innovation and technological challenges. 2013, *Advanced Engineering Materials*.
39. Wang S.W.. Aluminum Foam Stabilization by Solid Particles. *The Canadian Journal of Metallurgy and Materials Science*.
40. Haibel, A., Why are metal foams stable?. 2006, *Applied Physics Letters*.
41. Mahadev. A Review on Production of Aluminium Metal Foams. Mr., : 2018, *IOP Conf. Ser.: Mater. Sci. Eng.*
42. Eglero, J.A., Solórzano E., E. Design and Testing of an Energy Absorber Prototype Based on Aluminium Foams. R 2010.
43. Nakajima, H. Fabrication, Properties and Application of Porous Metals with Directional Pores. 2007, *Prog. Mater. Sci.* , pp. , 1091–1173.
44. Haesche, M., Lehmhus, D. And Weise, J. Carbonates as Foaming Agent in Chip-Based Aluminium Foam Precursor. 2010, *J. Mater. Sci. Technol.* , pp. 845-850.
45. Lehmhus D. Dynamic Collapse Mechanisms in Metal Foam Expansion. *Advanced Engineering Materials*.
46. Güner A. New Approaches to Aluminum Integral Foam Production with Casting Methods. 2015, *Metals*.

47. Nakajima H., Fabrication, properties and application of porous metals with directional pores. 2007, Progress in Materials Science .
48. Celal C., Niini E. Foamed aluminum parts by investment casting. 2009, Colloids and Surfaces A: Physicochemical and Engineering aspects.
49. Banhart, J., Metallic foams: challenges and opportunities.. 2000, Fraunhofer-Institute for Advanced Materials.
50. Branimir L., Sonja J., Jure K. 2021, Production of Open Cell Foams Out of Aluminium Chips. Y Athens Journal of Technology and Engineering , pp. Pages 299-310.
51. Yilmaz z., , aktemur s., buzoglu h., gümüsderelioglu m.,the effect of temperature and ph variations on the surface tension of edta solutions.. 2011, Journal of Endodontics.
52. Kulkarn. Density and viscosity study of binary mixtures of ethanol -water at different temperatures. 2013, science journal of pure and applied chemistry.
53. Liu H., Xie M.,. Three-dimensional CFD simulation of bubble–melt two-phase flow with air injecting and melt stirring. International Journal of Heat and Fluid Flow.
54. Dinsdale, a. T. The viscosity of aluminium and its alloys—a review of data and models. 2004, proceedings of the 2003 international symposium on liquid metals.
55. Wang D., Effect of ceramic particles on cell size and wall thickness of AL foam. 2003, Materials Science and Engineering, pp. 45 - 49.
56. K. Khattab i., Bandarkar F Density, viscosity, and surface tension of water ethanol mixtures from 293 to 323.,. Korean J. Chem. Eng.
57. Khattab i. Density, viscosity, and surface tension of water+ethanol mixtures from 293 to 323k. K 2012, korean j. Chem. Eng.

58. OZBAYOGLU, E. M. Image Processing Techniques in Foam Characterization. 2007, Energy Sources.
59. Zhou X. Quantitative characterization of uniformity of cells in aluminum foams. 2008, School of Metallurgical Science and Engineering, Central South University, Changsha 410083, China.
60. Nyarko, E.K. Glavaš, H. Determination of Foam Stability in Lager Beers Using Digital Image Analysis of Images Obtained Using RGB and 3D Cameras. 2021, Fermentation.
61. Versluis m., high-speed imaging in fluids. 2013, experiments in fluids.
62. Gadallah h., kamran. A., novel nozzle design for reducing bubble size generated in stagnant liquid. Siddiqui, aly 2013, asme fluids engineering division summer meeting .
63. Rodríguez b. Rising velocity for single bubbles in pure liquids. 2012, mexican journal of chemical engineering.
64. Jinsong H. Numerical simulation of bubble rising in viscous liquid. 2007, Journal of Computational Physics.
65. Gholamreza, K. Transient analysis of a single rising bubble used for numerical validation for multiphase flow. 2014, Chemical Engineering Science.
66. Colombo, P. Conventional and novel processing methods for cellular ceramics. 2005, Philosophical Transactions A.
67. Stochero N., Guzi de Moraes E. Influence of wet foam stability on the microstructure of ceramic shell foams. 2020, . .
68. Liu H., Xie M., Li K., Wang D., Three-dimensional CFD simulation of bubble–melt two-phase flow with air injecting and melt stirring. 2011, International Journal of Heat and Fluid Flow.

69. Rajak, D. Technical Overview of Aluminum Alloy Foam. 2007, Material Science 48.
70. Jamialahmadi M. Terminal Bubble Rise Velocity in Liquids. 1994, Chemical Engineering Research and Design.
71. Ma, Z.H. compressible Multiphase Flow Model for Violent Aerated Wave Impact Problems. 2017, Proc. R. Soc. A vol. 470.
72. Gumulya, M. Bubbles in viscous liquids: Time Dependent Behaviour and Wake Characteristics. 2016, Chemical Engineering Science.
73. Krull B., Strumpf E., Keplinger O., Shevchenko N., Fröhlich, J., Eckert. Combined Experimental and Numerical Analysis of a Bubbly Liquid Metal Flow. 2017, Materials Science and Engineering 228.
74. An X., Kou J., Qiao Z., and Sun S., A Componentwise Convex Splitting Scheme for Diffuse Interface Models with Van der Waals and Peng–Robinson Equations of State. F. 2016.
75. Fluent, ANSYS. Help Manual, Chapter 21.1.2. 2020.
76. Menter, F. R. Two Equation Eddy-Viscosity Turbulence Models For Engineering. 1994, AIAA journals.
77. Nova I., Fraňa K. , Solfronk P., Korecek D. Monitoring the Influence of Sodium Chloride Particle Size on the Physical, Mechanical Properties and Structure of Samples of Porous aluminium materials. 2021, manufacturing technology.
78. Yilmaz z1, aktemur s, buzoglu hd, gümüsderelioglu m. The effect of temperature and ph variations on the surface tension of edta solutions. 2011, journal of endodontics.
79. Perego, C., Microporous and Mesoporous Materials. 2013, The Official Journal of the International Zeolite Association.

80. Holland, B.T. Synthesis of Macroporous Minerals with Highly Ordered Three-Dimensional Arrays of Spheroidal Voids. 1998, *Science* 281.
81. Bacterial templating of ordered macrostructures in silica and silica-surfactant mesophases. Davis, S.A. 1997, *Nature*.
82. Marcos-Hernández M., Mesoporous Composite Nanomaterials for Dye Removal and Other Applications. *Composite Nanoadsorbents*.
83. Laurie. J., *Non-Cryst. Solids*. 1992.
84. Ma Z.H., Causon D.M., Qian L., Mingham C.G., Gu H.B., Martnez Ferrer, A compressible Multiphase Flow Model for Violent Aerated Wave Impact Problems. P. 2017, *Proc. R. Soc. A* vol. 470.
85. Biological systems engineering. [Online]
<http://sites.bsye.wsu.edu/pitts/be120/Handouts/animal%20tssue%20descriptio ns%20and%20mechanical%20proprties.htm#:~:text=The%20ligament%20or %20tendon%20then,produce%20the%20ligament%20or%20tendon..>
86. Wang J., Wang H., Wang K., Ice crystals growth driving assembly of porous nitrogen-doped graphene for catalyzing oxygen reduction probed by in situ fluorescence electrochemistry. (2014), *Sci Rep* 4.
87. Oeffner J., The Hydrodynamic Function of Shark Skin and Two Biomimetic Applications. 2012, *Journal of Experimental Biology*.
88. Banhart J., Seeliger H., Recent trends in aluminum foam sandwich technology. -W. 2012, *Adv. Eng. Mater.*, Vol. 14, pp. 1082–1087.
89. García-Moreno F., Commercial Applications of Metal Foams: Their Properties and Production. 2016, *Materials*.
90. Hooker, H. <https://www.photoblog.com/learn/photography-histogram/>. [Online]

91. Kulshreshtha A., Preparation of metal foam by different methods: A review. 2020, Materials today proceedings, Vol. 26.

92. Heim K., “Particle size and fraction required to stabilise aluminium alloy foams created by gas injection,” Scripta Materialia, 2018.

Appendix 1 – CFD Air Bubble volume fraction contours:

Photos are arranged in chronological order

| | |
|------------------|------------|
| Nozzle Diameter | 3 [mm] |
| Volume flow rate | 130 [l/hr] |
| Surface tension | 72 mN/m |

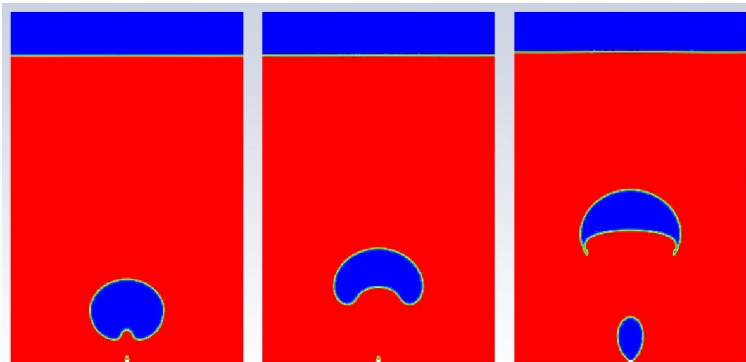


Figure 72 First bubble leaving the nozzle

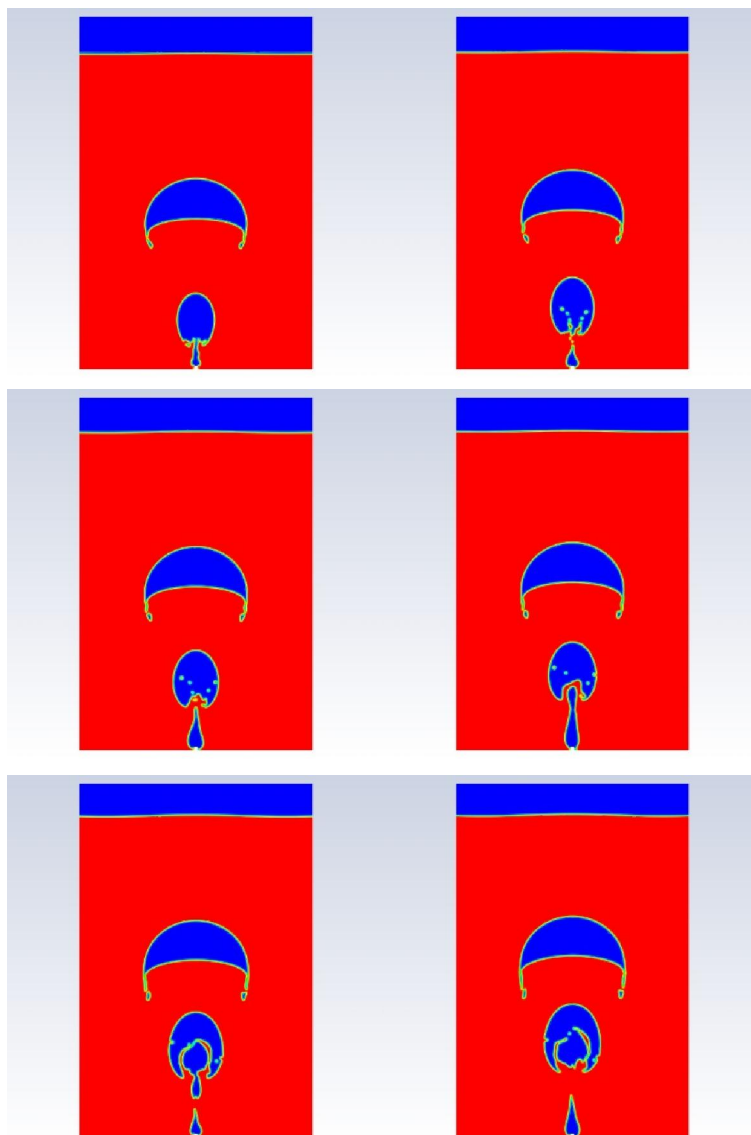


Figure 73 bubble coalescence

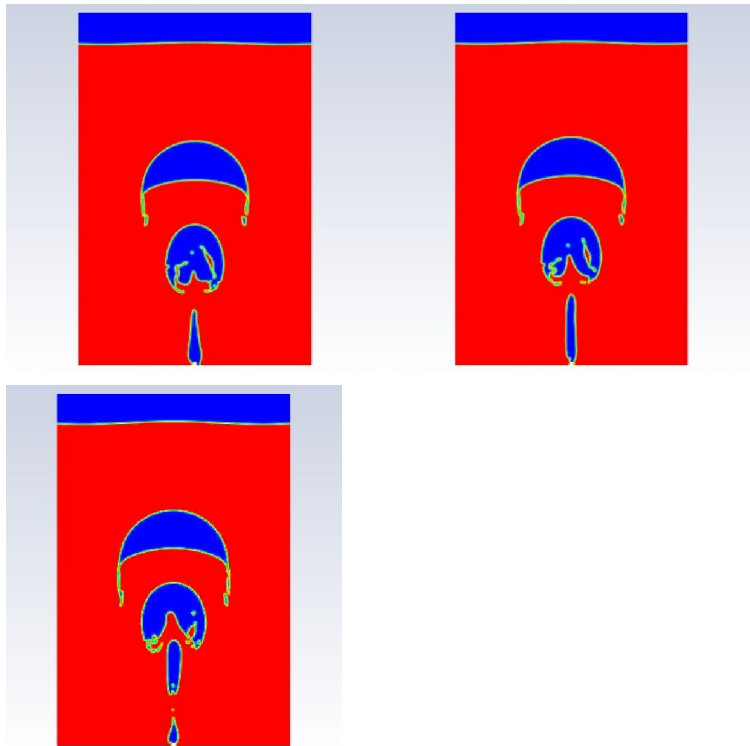


Figure 74 mid tank height area, bubble experience a slowdown in velocity

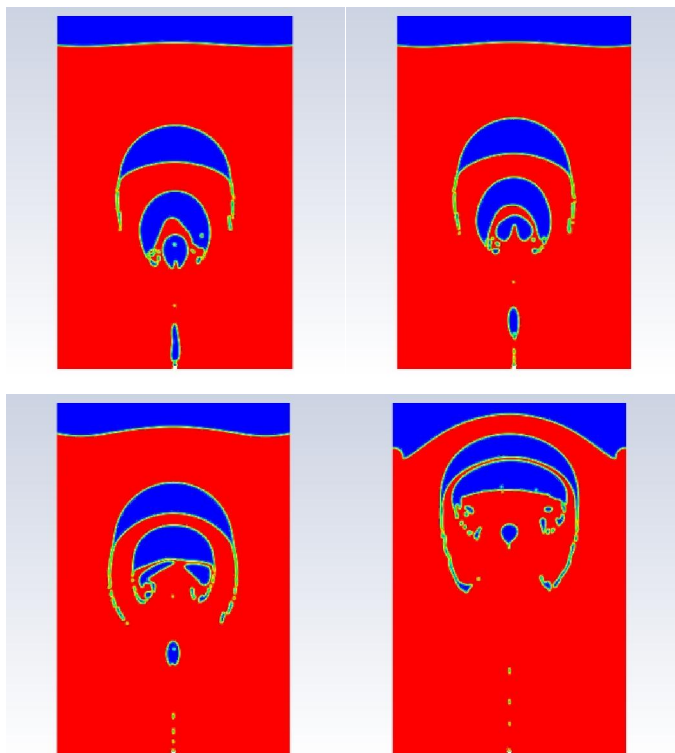


Figure 75 breaking out of the surface

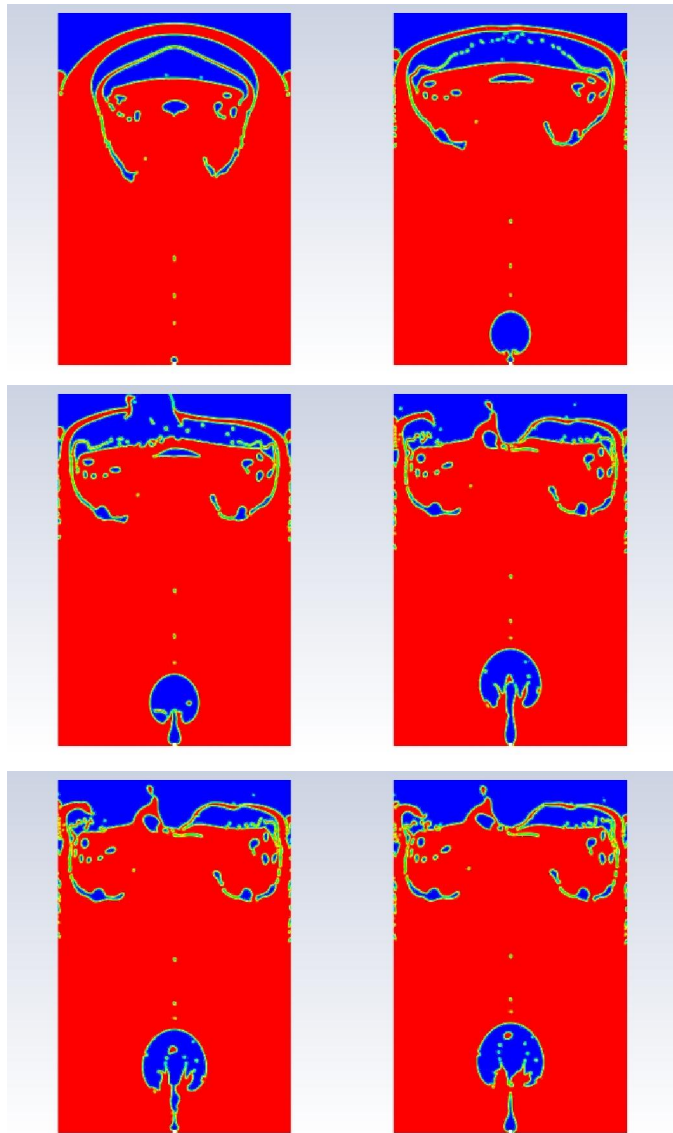
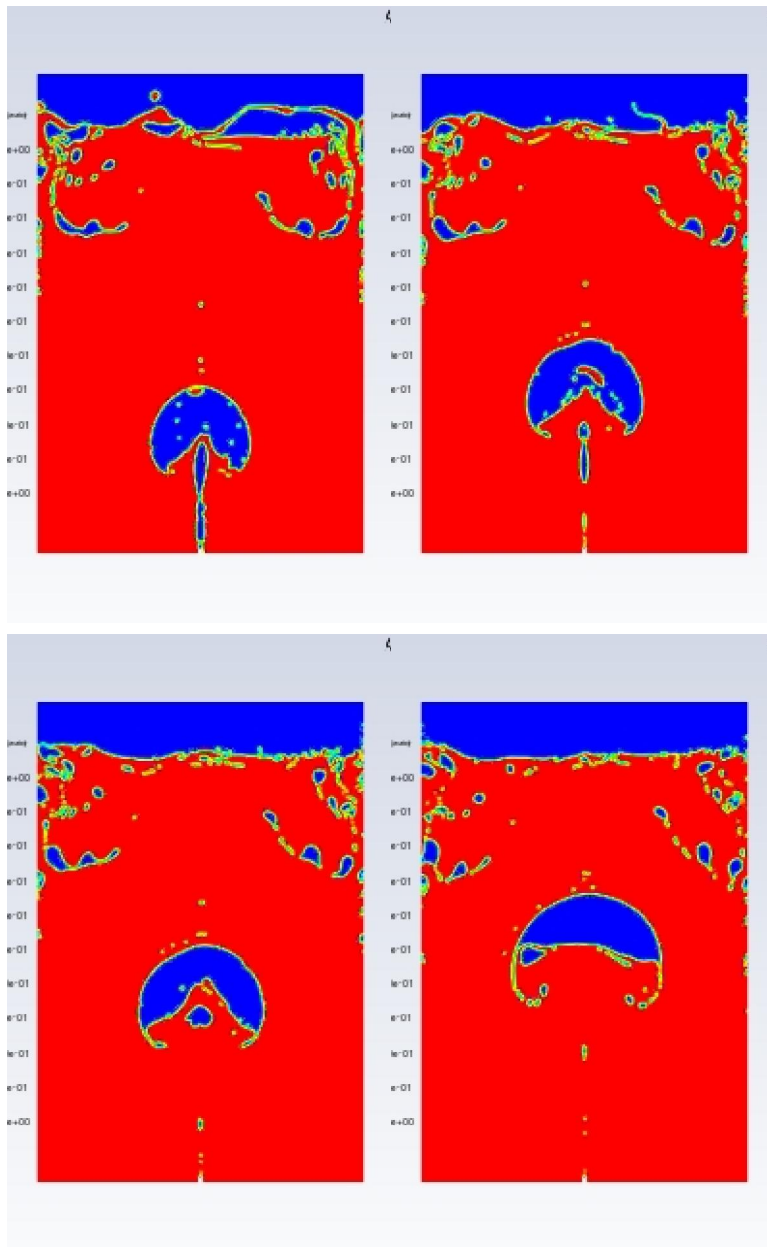


Figure 76 turbulence created by breaking the surface already affects the generating of new bubble



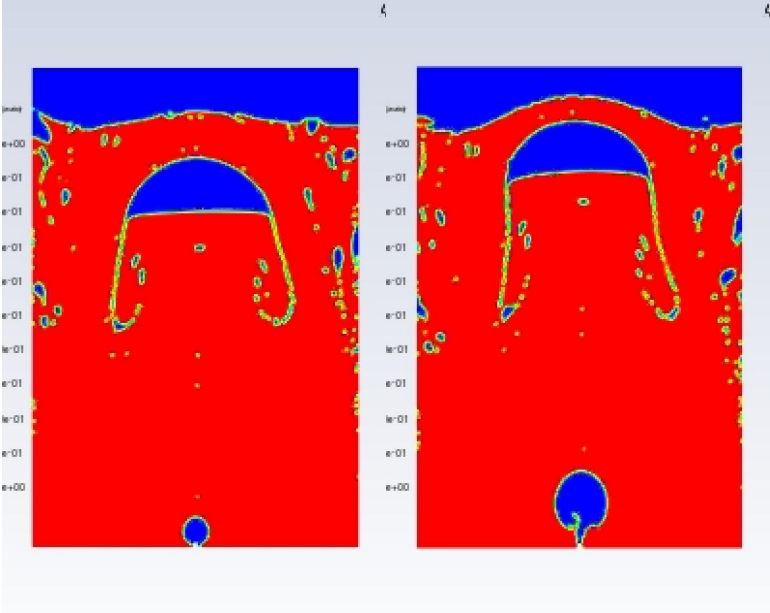


Figure 77 due to high turbulence, second wave of bubbles have a different pattern of coalescence

Appendix 2 – High Speed Camera Air Bubble photos:

Speed camera photos sorted chronologically

| | |
|------------------|------------|
| Nozzle Diameter | 3 [mm] |
| Volume flow rate | 120 [l/hr] |
| Surface tension | 72 mN/m |

